QATAR UNIVERSITY

COLLEGE OF ENGINEERING

INVESTIGATING FATIGUE LIFE IN BOLTED FLANGE CONNECTION IN WIND

TURBINE TOWERS

BY

ABDULLAH M. SALAMEH

A Thesis Submitted to

the College of Engineering

in Partial Fulfillment of the Requirements for the Degree of

Masters of Science in Mechanical Engineering

June 2023

COMMITTEE PAGE

The members of the Committee approve the Thesis of
Abdullah M. Salameh defended on 04/06/2023.

_____

Dr. Jamil Renno
Thesis Supervisor

_____

D r. John-John Cabibihan
Program Coordinator

_____

Dr. Mustafa Arafa
Committee Member

_____

Dr. Sadok Sassi
Committee Member

_____

Dr. Mohammad Paurobally
Committee Member

_____

Approved:

_____

Khalid Kamal Naji, Dean, College of Engineering

ABSTRACT

SALAMEH, ABDULLAH, M., Masters: June: 2023, Master of Science in Mechanical Engineering

Title: Investigating Fatigue Life in Bolted Flange Connection in Wind Turbine Towers

Supervisor of Thesis: Dr. Jamil Renno

A comprehensive assessment of fatigue was performed on an L-flanged bolted connection under four different wind speeds. The wind turbines were subjected to average wind speeds of 5, 10, 15, and 20 m/s. The primary objective was to investigate how the fatigue life was influenced by increasing the number and size of bolts while also developing a systematic approach for analyzing the fatigue life of bolted flange connections more broadly. The study determined that increasing the size or number of bolts can notably improve the fatigue life of bolted flange connections. Additionally, the curves derived from the assessment data demonstrated a steeper slope for a greater number of bolts, indicating that the percentage increase of adding bolts is not consistent for each additional bolt. Instead, the percentage increment rises exponentially when increasing the number of bolts. However, selecting the most suitable design improvement strategy depends on the specific circumstances. For example, increasing the number of bolts may not always be possible due to spatial limitations. In the majority of cases, the study observed that increasing the number of bolts resulted in significant improvements in fatigue life, regardless of the size of the bolts used. This noteworthy finding can be particularly advantageous when assessing the cost-effectiveness of possible solutions for enhancing the durability of bolted flange connections.

DEDICATION

I dedicate this thesis to my family and friends, who have consistently supported and motivated me with their warm prayers and kind words, enabling me to achieve my goals. I would like to express my sincere gratitude to my supervisor, Dr. Jamil Renno, for his unwavering guidance and support throughout my master's journey. Without your constant support and guidance, I would not have achieved this success. Thank you all for being an essential part of my life.

ACKNOWLEDGMENTS

TABLE OF CONTENTS

LIST OF TABLES

LIST OF FIGURES

CHAPTER 1: INTRODUCTION

The introduction chapter contains background about the studied topic followed by the research objectives, and significance. Furthermore, the complete thesis outline will be presented at the end of this chapter.

1.1. Background

In recent years, renewable energy sources have received increased attention as a reaction to the difficulties presented by climate change, energy security, and the need for sustainable energy supplies. In response to increased interest, the literature on renewable energy and associated devices has developed fast, providing significant insights into the development and deployment of these technologies.

Figure 1. The main kinds of renewable energy sources [1].

Solar energy is one of the most commonly investigated and used renewable energy sources. Many studies have been conducted to investigate the technical and economic aspects of photovoltaic (PV) technology, such as the design and optimization of PV panels [2] and the integration of PV systems into the current electrical grid [3]. Besides this, research has focused on the social and policy elements of solar energy, such as public perception and acceptability of PV systems [4] and the role of government in supporting solar energy adoption [5].

Wind energy is another rising field of renewable energy, with a concentration on wind turbine design and optimization [6]. Wind energy integration into the current electrical grid has also been studied, as well as the influence of wind energy on local populations [7].

Hydro energy is a recognized renewable energy source, with an emphasis on improving the efficiency and dependability of hydroelectric power facilities [8]. The influence of hydro energy on local communities has also been studied [9], along with the integration of hydro energy into the current electrical infrastructure.

Geothermal energy is an emerging renewable energy source that focuses on the discovery and exploitation of geothermal resources [10]. The technical and economic elements of geothermal energy have also been studied, including the design and optimization of geothermal power plants [11] and the integration of geothermal energy into the current electrical grid.

Biomass energy is a type of renewable energy that has gained popularity in recent years, with an emphasis on the conversion of biomass into energy [12]. The sustainability and environmental effect of biomass energy have also been studied [13], along with the integration of biomass energy into the current electrical system [14].

Eventually, the literature on renewable energy and related devices is a wealth of knowledge on the technical, economic, social, and policy aspects of these technologies. These studies have demonstrated that renewable energy technologies have the potential to deliver clean, sustainable, and cost-effective energy, as well as the significance of ongoing research and development to enhance their performance and adoption.

The general idea of the wind turbine has been initiated back in the 19th century when it was commonly used to pump water and grind grains. Moreover, the technology of the wind turbine has been developed, and nowadays, wind turbines are commonly used to generate power like electricity. Next, the lights will be spotted on the working method of the turbines during the past.

One of the earliest records of using wind turbines was spotted in the Persian community, where they used windmills to pump water [15]. The preliminary design of the wind turbines has been improved over the next centuries, and by establishing the multi-bladed turbines by end of the 19th century till that time, turbines were commonly used to pump water and grind grains.

During this time, the technology of wind turbines continued to improve especially in the 20th century by producing large multi-megawatt wind turbines. As stated in the references, the first modern wind turbine was developed back in the 70s and 80s in the last century mainly in distant areas where the electrical grids were not yet in service [16]. From that time, the turbine's technology kept developing by delivering more efficient and reliable turbines, and in 2020, wind turbines covered 16% of overall EU electricity demands [17].

The main working concept of the wind turbine is by enhancing the captured wind's energy and converting it to rotational energy. Then by rotating the blades which are connected to a generator, the electricity will be generated. The main intention of designing any wind turbine is aerodynamics which mainly affects the capturing of the wind's energy over the blades. Blades are considered the most important part of the wind turbine since they have the main role of rotating due to the conversion of the wind energy to rotational energy for electricity generation. The blade's design is sized based

on several factors like speed, wind direction, shape, and the dimension of the blades and the blade's raw material [18].

As the world continues to adopt innovation and develops renewable energy sources, wind turbines become of implementing innovation and developing renewable energy sources, wind turbine starts gradually more popular as an electricity source. There are several types of wind turbines that have been used for the time being, and in this part, the types of wind turbines and their characteristics will be compared.

The first type of wind turbine is the horizontal-axis wind turbine "HAWTs". In this type of turbine, the rotor is mounted on the horizontal axis. HAWTs are the most commonly used type among all types of wind turbines. Also, They can be used in small and large end energy systems [19]. Furthermore, the HAWTs have two sub-categories, upwind turbines, and downwind turbines. For the upwind turbines, the wind will face the trailing edge of the blades. On the other hand, in the downwind turbines, the wind will face the leading edge of the blades [16].

The other type of wind turbine is referred to as a vertical-axis wind turbine "VAWTs". In this type of turbine, the rotor is mounted on the vertical axis. Compared to HAWTs, the VAWTs are less common and mainly used in small-size energy systems since they are more compact and have a lower cost [18]. Moreover, the VAWTs have two sub-categories, Darrieus turbines, and Savonius turbines, and the main difference is the blade shape. In the Darrieus turbines, the blades will be like airfoils and in Savonius turbines, the blades will have a cylindrical shape [15].

An additional type of wind turbine can be referred to as a tubular turbine, where the rotor is mounted in the cylindrical tower and the blades are perpendicular to the rotation's axis. Compared to HAWTs and VAWTs, the tubular turbine is less common

and it is mostly used in small-size energy systems because its maintenance is simple and cheap. In general, there are numerous types of wind turbines in addition to HAWTs, VAWTs, and tubular turbines, and each type can be selected based on the application to implement it is specified characteristics in the wind energy system.

Wind turbines might seem an easy and powerful machine to produce clean energy, but it requires a lot of studies to select the location, in addition to its environmental impact. These constraints are the major reason to limit the usage of wind turbines and deviate to alternative methods in some regions.

A thorough study must be conducted in order to select the location of a wind turbine as it cannot be built into any environment. This goes back firstly to the basic concept of a wind turbine, which is the wind. Thus, it is required to have the wind with high speed, consistent and reliable flow. For example, in coastal areas or oceans wind is strongest and most consistent [20]. Moreover, the reliability of the wind can eliminate a location as it is unpredictable if it significantly varies every hour, day, and season, hence, the energy to be produced from a wind turbine cannot be predicted precisely to meet the required amount [21]. In addition, these wind conditions can be met in some regions but still, the wind turbine cannot be built there if the area is not compatible. Not accessible for maintenance is an example or nonutilitarian ones or even the soil is not reliable.

On the other hand, it cannot be built in an area that might cause a threat to the environment. For instance, displacement of the surrounding wildlife or birds' migration pattern [22]. Furthermore, soil erosion might occur where the wind turbine is going to be constructed, hence, it will disturb the ecosystem.

To sum up, producing clean and renewable energy with a wind turbine is a great concept but there are some constraints that can oppose the development of this industry.

This includes the selection of the location considering the wind characteristics, wind reliability, and compatibility of the area. Moreover, the disruption of the surrounding habitats, environment, and land shall be taken care of.

Utilizing wind energy into converting it into electricity requires complicated and sophisticated concepts that are implemented into a rotor, generator, control system, tower, and foundation to assemble a wind turbine. Thus, this literature reviews each component of a wind turbine. Achieving so would enhance the understanding of each part's design and function, which would result in generating new innovative ideas to optimize the system. However, all parts are equally important in their own way, and developing any would result in more efficient performance.

To begin with, the most common part is the rotor which is shown in Figure 2 is the component that is responsible for converting wind energy into kinetic energy.

Figure 3: Blades aerodynamic profile [24]

Figure 2: The blades and the rotor [23]

The wind would hit the blades to rotate the weight of the rotor to create kinetic energy. The blades' aerodynamic profile aims to utilize the maximum wind energy into maximum kinetic energy [25]. Thus, the profile of the blades, their number, length, and the weight of the rotor are key characteristics. Consequently, every slight detail in the

design can affect the performance of the system [26].

Secondly, the generator is the device that converts the kinetic energy produced by the rotor into electrical energy [27]. Figure 4 shows the generator and its location in the wind turbine.

Generator
Electrical Asymmetries
Overheating
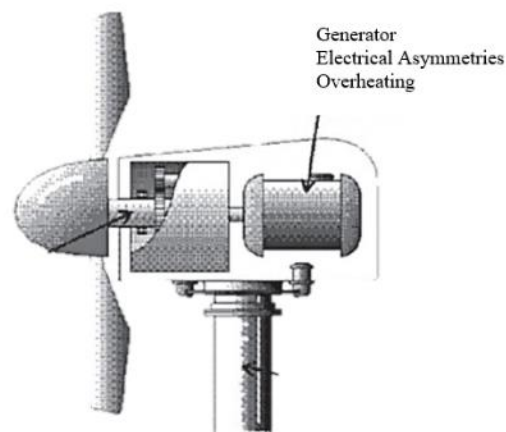
Figure 4. Cross-sectional view of a schematic diagram of a wind turbine showing the generator [28]

Thus, as the generator is the core purpose of the wind turbine, there are various concepts of it. To name a few, there are induction and permanent magnet generators. However, the design criteria of the wind turbine would specify the type of generator with all its specifications [29].

Thirdly, the control system functions as the brain of the whole wind turbine. Its power is supplied by the generator, but it invests this electrical energy into enhancing the overall efficiency of the machine. Figure 5 shows the diagram of the control system in wind turbines.
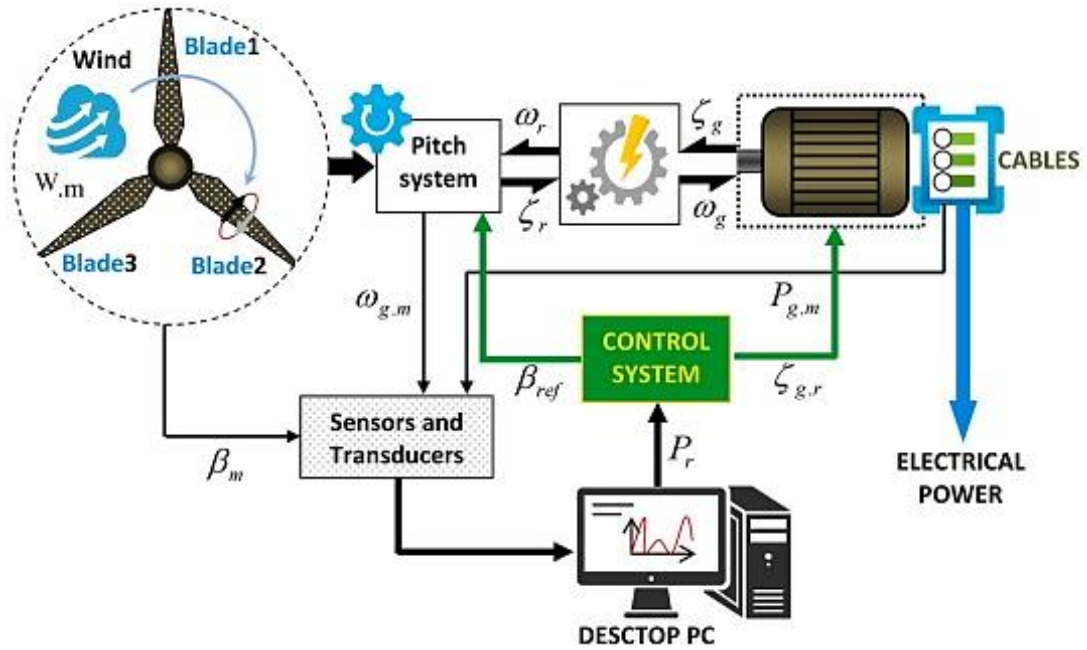
Figure 5. Control system diagram [30]

It can adjust the angle of the rotor's blade in order to attain as much wind energy as possible. Moreover, it is connected to several types of anemometers to analyze and control the performance according to their measurements of the wind direction and speed. Finally, it constantly measures the efficiency of the wind turbine and ensures that it is operating safely [31].

Fourthly, the tower structure or the beam that is carrying all these components together against all the static and dynamic loads is the tower. Figure 6 shows the most significant loads applied on the tower.
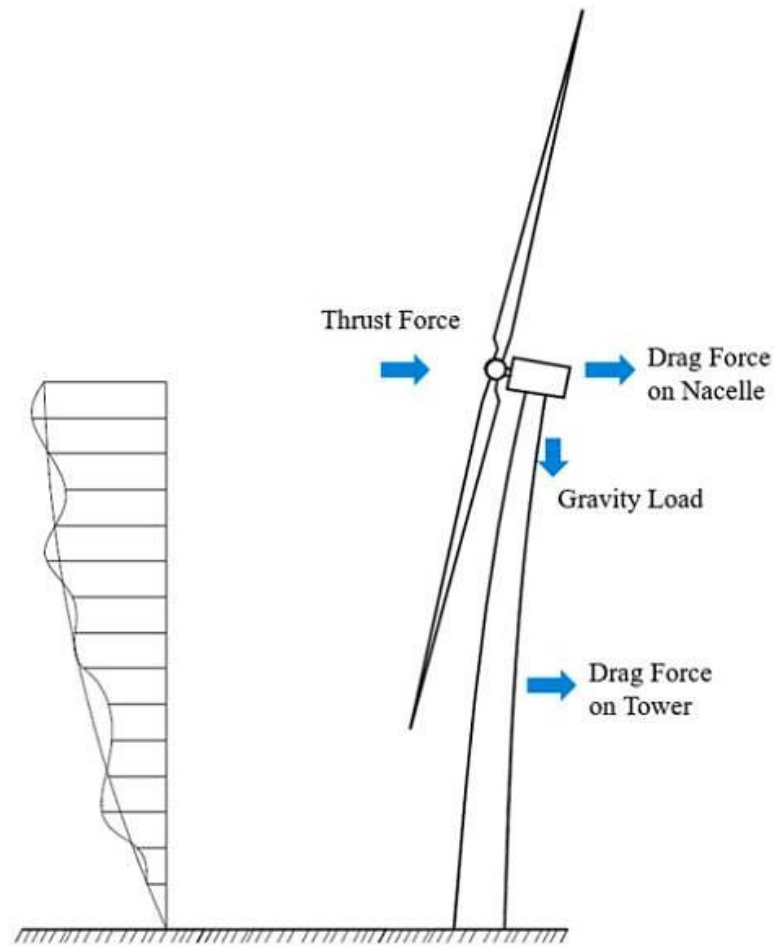
Figure 6. Schematic diagram of the forces acting upon the tower [32]

Therefore, the major characteristic of the tower is to be strong and stable [33]. However, the design specifications of the wind turbine narrow down the options for selecting the materials the tower would be made from [34]. For example, the tower can be built from fiberglass steel or concrete. Nevertheless, the tower's design might seem to have no major function to the wind turbine except for supporting the rotor, it evidently can impact the wind turbine's total efficiency, reliability, and safety [34].

Finally, the function of a foundation in a wind turbine is to hold the structure and counter some dynamic loads in a few cases.
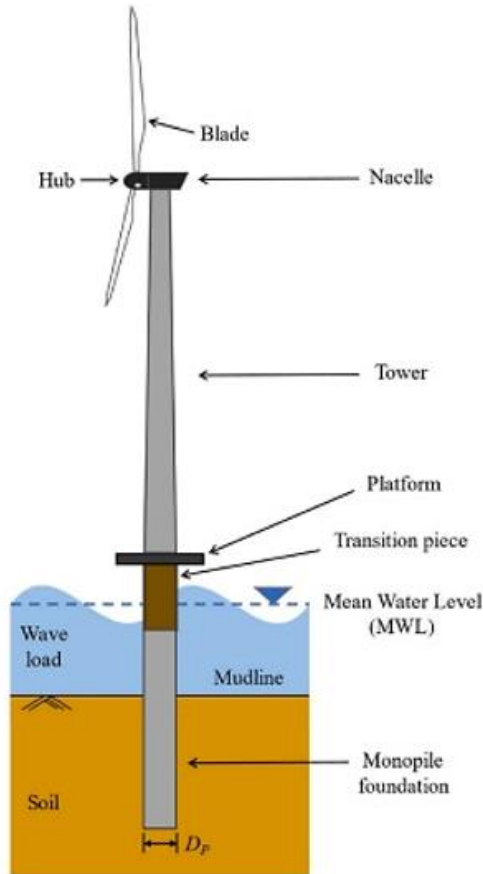
Figure 7: Schematic diagram of an offshore foundation [35]

Figure 8: Schematic diagram of an onshore foundation [36]

If the wind turbine was offshore, it can be equipped with a floating platform, otherwise, it is designed based on the type of soil and local regulations to be a slab [25]. Consequently, the design of the foundation can significantly affect the total efficiency and cost of the wind turbine [29]. Figure 7 and Figure 8 show both types of foundations.

In conclusion, the rotor converts the wind energy into kinetic energy, then the generator transfer that into electrical energy under the adjustments of the control system based on the wind speed and direction. The tower and the foundation are also major components in the system and can impact its total efficiency as they mount in a reliable and safe manner. Thus, studying the major components of the wind turbine and the function of each can develop creative ideas to optimize the total performance.

The plate that connects the ends of the tower sections is called the flange which is shown in Figure 9 and Figure 10. Also, it is designed to be a metal part to withstand various loads such as rotor loads, wind loads, and other dynamic loads. Correspondingly, the flange also must provide a stable surface for the gusset plate to be attached to [37]. Therefore, the flange is a crucial component in the design and functioning of wind turbine towers. The gusset plate can be defined as an additional metal plate to afford structural support to the tower connections. Similarly, the design of the gusset plate depends on the loads it must withstand including the previous loads mentioned [38]. The flange bolts are used to provide a secure connection and they have to be designed strong enough to resist the loads discussed, which will play a significant role in the overall stability and reliability of the wind turbine tower [39].
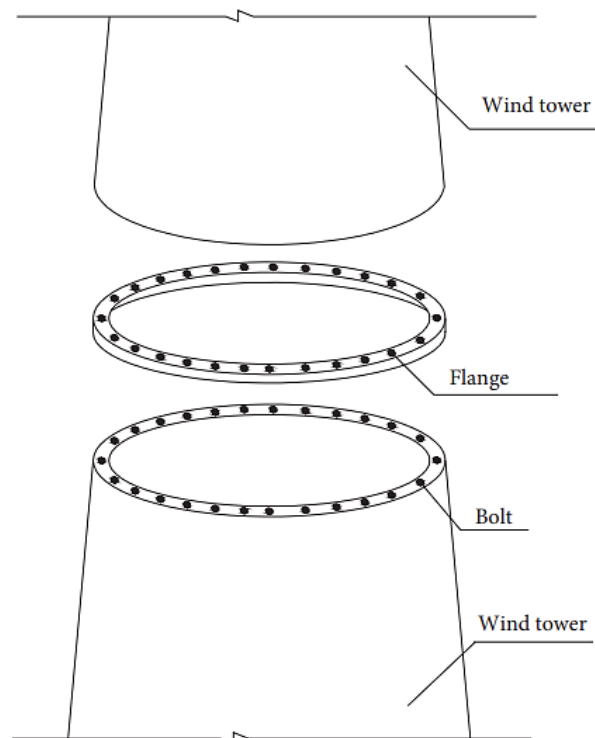
Figure 9. Flange connection of wind tower [40]

Figure 10. Detail of flange and bolts [41]

Flange connection failure can lead to substantial damage to the wind turbine tower and its components and can have serious consequences for the overall system. Material defects by using poor quality material or improper manufacturing processes are considered one of the main causes of flange connection failure and may lead to flange connection break [37]. Material degradation over time due to exposure to extreme weather conditions or corrosion can also contribute to flange connection failures [39].

Improper installation procedure such as poor alignment or incorrect bolt tightening is another cause of flange connection failure, which could increase the stress on the connection in addition to breaking the flange connection [42] [43].

Another significant factor that causes flange connection failure is high loads. For instance, heavy loads because of strong winds lead to breaking the flange connection [39]. Furthermore, improper load distribution and inadequate load analysis can contribute to flange connection failures [42].

Fatigue failure in wind turbine tower flange connections can also be the result of improper maintenance and inspection practices. Regular maintenance and inspections can help to identify and address potential fatigue issues before they result in failure [44].

In conclusion, wind turbine tower flange connection fatigue failure can have serious consequences for the overall system and its components. To minimize the risk of fatigue failure, it is important to ensure proper design and manufacturing practices, conduct regular maintenance and inspections, and continuously monitor and assess the loads and environmental conditions experienced by the flange connection.

1.2. Research Objectives

The aims of this research are as follows:

1- To investigate the effect of number of bolts in flanged connection on the fatigue life for 5MW wind turbines.

2- To study the effect of size of bolts in flanged connection on the fatigue life for 5MW wind turbines.

3- To design a systematic methodology of studying the fatigue life of bolted flange connection in general.

1.3. Significance of the Research

Since the world's vision is to move to renewable energy such as wind, studying all the aspects of the wind turbine is required. One of the most significant aspects of wind turbines is structure strength. The structures of wind turbines are subjected to high dynamic forces mostly caused by wind. As a result, studying the fatigue life of the structure bolted connection is significant to ensure its safety and reliability. Furthermore, Flanged connections are widely used among many applications other than wind turbine towers, such as electric poles which are also subjected to wind load. Suspension and steering systems in automotive applications are also subjected to dynamic loads.

1.4. Thesis Layout

This thesis will include five different chapters. Chapter 1, which is introduction will provide information about renewable energy, wind turbines, turbine parts, and failure mechanisms of turbine flange. Chapter 2 will contain some literature reviews about wind turbines. Chapter 3 will include a comprehensive description of the methodology used in this thesis. Finite element analysis and other software results with discussion and analysis will be carried out in chapter 4. Lastly, chapter 5 will present the findings of this thesis.

CHAPTER 2: LITERATURE REVIEW

Chapter 2 provides different details about fatigue, loads, stresses, and bolts in wind turbines. In addition, more formulas, figures, and existing studies are provided to review, explain, and clarify the concerned problem in this thesis. Lastly, brief literature is given about the software and codes that were useful in this thesis.

2.1. Assessing the Fatigue Behavior Problem of Bolting Connections

Wind turbines contain ring joints that are L-flange shaped [45]. Numerous bolt assemblies that are high-strength and organized circumferentially make up these ring joints [46]. Bolts in the joints have a geometric alignment and are made up of bolts, washers, and nuts. Moreover, the bolts are tightened by clearly defined preloading conditions. Understandably, the bolting assemblies that are preloaded are usually tightened to a specified minimum force level. The tightening is conducted by clearly identified installation procedures. Preloading the connections is critical for their structural stability and reliability [47].

The process of preloading the joints is usually effectively conducted using the torque technique. In the torque technique, a hydraulic wrench is employed in tightening the nut until a given torque point is attained [48]. Implementation of this procedure follows guidelines that have nominal preload values. Guidelines must be adhered to for safe and high-quality fastening as well as the prevention of plastic deformations.

For simplicity, it is vital to make the analysis on the maximum loaded flange segment of the connections, which will provide valuable insight for determining the dimensions of the bolts as shown in Figure 11. In the diagram, the left section illustrates the tower part procedure used to design L-flange connection rings whereas towards the

right of the image is the illustration of the load transfer schematic demonstration.
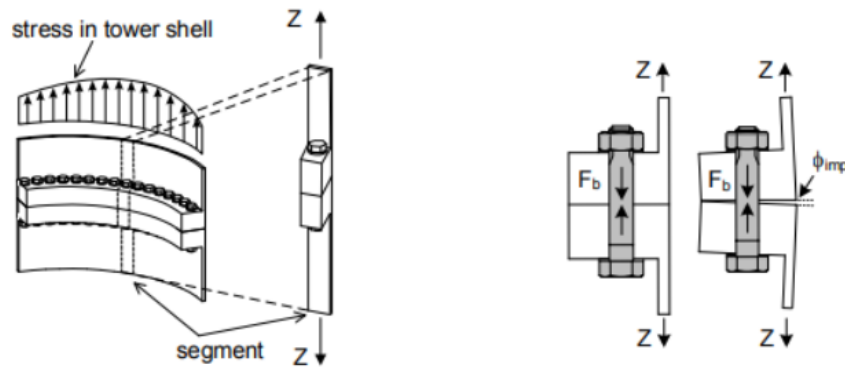
Figure 11. Ring L-flange connection [46] and transfer load description [49]

Axal load contribute mainly to the load in the ring L-flanges [49]. However, some load is derived from the bending which occurs as a result of the existence of eccentricity in the middle of the tower shell and the axis of the bolt. Non-linear load shifting conduct which exists in the middle of the tensile force Z (within tower shell part) and resultant bolt force $F_{b,}$ is a product of the preloading and eccentric geometry [46][50].

2.1.1 The Signs of Damaged Fatigue

Various features are symptomatic of fatigue damage. Engineers for wind turbines must be able to identify such characteristics so that they proactively tell when corrective action is needed [51]. With continued subjection to cyclic loading, metals tend to fail at load points that are substantially below their static strength level. The failure of metals at load levels below their static strength because of continued subjection to cyclic loading is caused by fatigue. For illustration purposes, the fatigue strength of a structural item is substantially lowered by the notch effect. Equally, the notch effect of thread renders bolted joints highly susceptible to fatigue strength damage. Taking the example of a fully loaded bolt, the flow of stress leads to peak

16

stress concentration within the pitch of the thread that is fully loaded; as illustrated in
Figure 12.
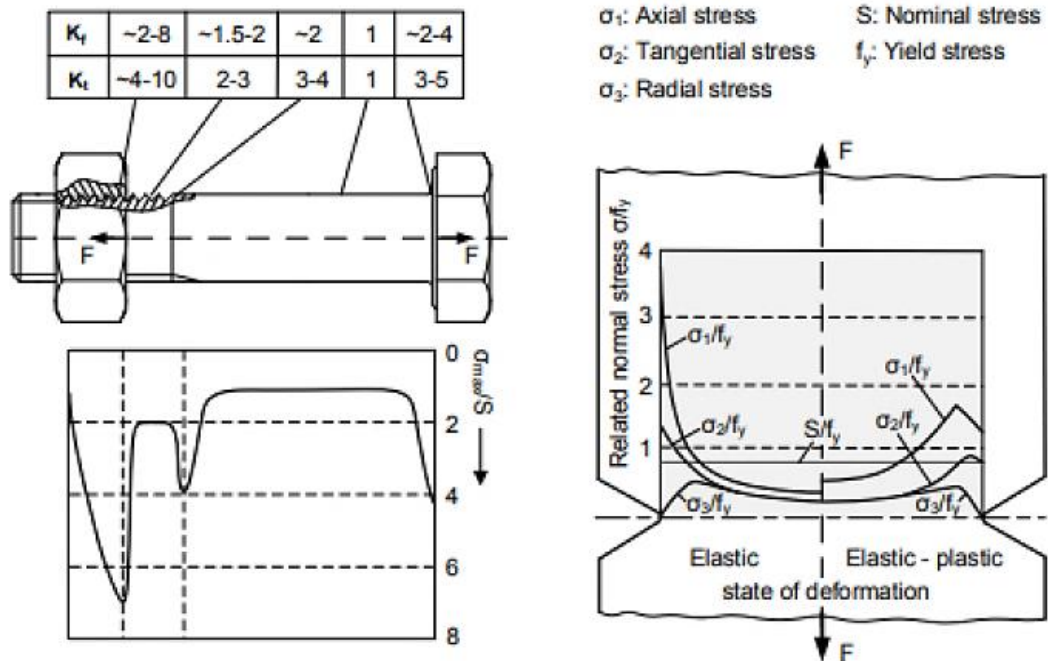
Figure 12. Strength distribution within the bolt-nut and the 3 types of axial stress [46]

Essentially, the notch stress building denoted as K_t is the nexus between optima local stress α_{max} and S, its nominal stress [52]. K_t may also give the quotient of linear elastic stress pile over geometric coordinate ξ [46]. Thus;

$$K_t = \frac{\sigma_{max}}{S} \ or \ K_t\left(\varepsilon\right) = \frac{\sigma(\varepsilon)}{S} \qquad (1)$$

Various types of stress develop when a bolted metal is subjected to axial loading. The notable stress types which develop under this condition include the state, tangential, and radial stresses [52]. The stresses usually build in the thread [53]. Notably, the stresses tend to remain inconsistent across the cross-section. It, thus,

implies that the material surrounding the bolt joint provides a supporting impact especially when the notch root is critically loaded above its fatigue strength [54]. There may be a redistribution of stress because the bolt material is ductile under local plasticity. The described behavior puts the fatigue strength of notched material always higher than expected for the notch stress pile which is the only one dependent on geometry [55]. The occurrence is denoted by the fatigue notch factor, K_f [53][54]. K_f is the result of dividing the fatigue limit of the constant amplitude in a metal that is not notched by the nominal stress sustainability limit in the notched part of the same material [52]. In this calculation, the geometric support impact is denoted by n_α. Thus;

$$K_f = \frac{\sigma_{a,D(kt=1)}}{S_{a,D(kt>1)}} = \frac{K_t}{n_\sigma}, with\ n_\sigma \geq 1 \tag{2}$$

2.1.2 Curves in Fatigue

Understandably, the S-N curves can be used to denote the fatigue strength of the structural parts and dimensions that are dependent on the level of the load. As shown in Figure 13, a logarithmic scale is applied in plotting sustainable load cycles up to failure, N, versus nominal stress amplitudes, S_α [56]. The former can also be plotted against the stress ranges. The described type of plotting is true in harmonic constant amplitude loading. The S-N curve has the advantage of enabling the division of the sustainable load cycle into different parts [57][58].
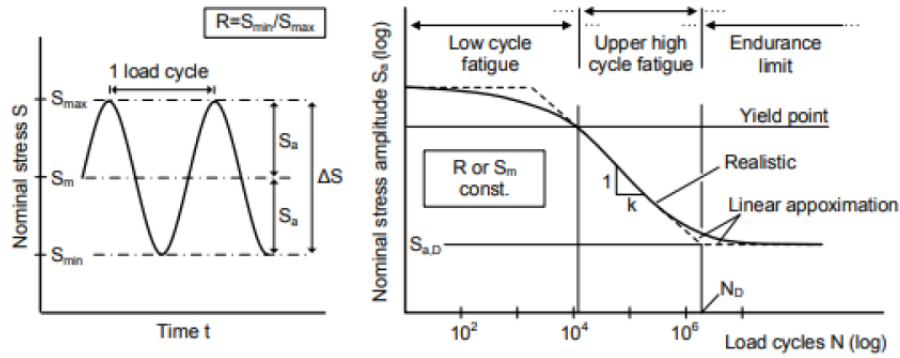
Figure 13. Typical values of loading in harmonic constant amplitude and the shape of the S-N curve [46]

Bolted assemblies for service loading in wind turbines feature non-constant amplitudes and stochastic sequences [59]. In this case, it is possible to convert load cycles in a given sequence to a sum of load amplitudes with the application of suitable algorithms. The scenario is illustrated in Figure 14. The conversion results in the loss of information regarding the pattern in cyclic loads succession [60]. Miner's rule is the most commonly applicable analytical model for estimation used. The rule is premised on the assumption that the overall damage of fatigue, D, is cumulative of the segment damages. Thus;

$$\sum_{i=1}^{i=n} D_i = \sum_{i=1}^{i=n} \frac{n_i}{N_i} \qquad (3)$$
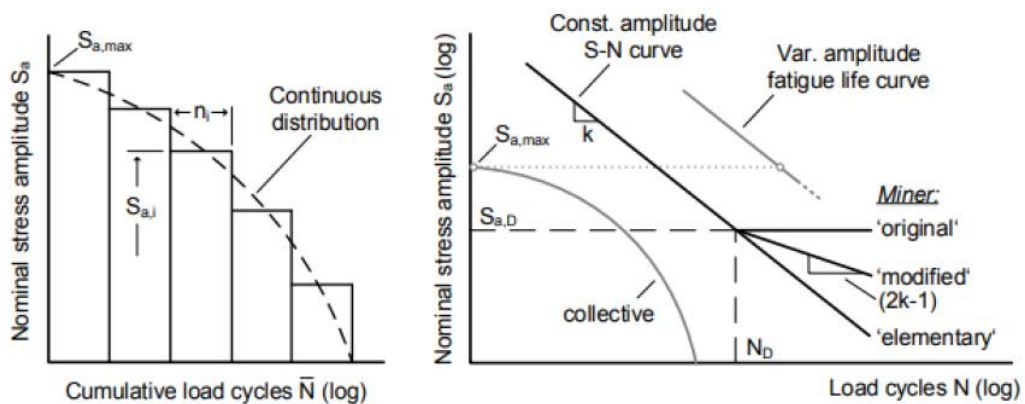
Figure 14. Discrete and continuous types of a load collective and Miner's rule various fatigue forms [46]

Fatigue refers to the process by which damage accumulates in bolted assemblies, as a result of the recurrent application of loads including the one below the threshold yield strength of a given metal [59]. Fatigue is characterized by the development of cracks, which continue to grow on every loading [54]. Figure 15 illustrates the preliminary progression of the fatigue crack.
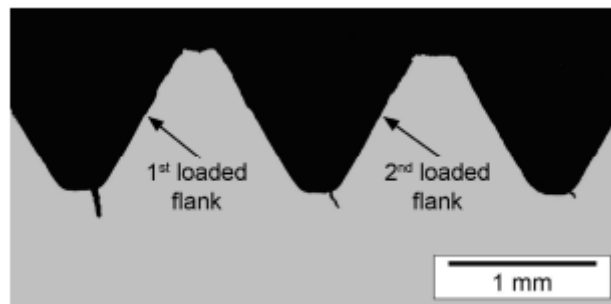
Figure 15. Initial progression of the crack in fatigue [54]

Fatigue failures or cracks exist in three main areas depending on the stress concentration [53]. Figure 16 illustrates this phenomenon. Almost 65% of fatigue cracks occur in the root of the first loaded thread, location 5 in this figure [61]. When materials are subjected to cyclic loading, dislocation motions within the areas of local stress concentration start the fatigue process, producing slip bands parallel to the highest alternating shear stresses. When the alternating load rises, the number of slip bands that are being made as incursions or extrusions on the material surface increases [55]. The micro-cracks tend to nucleate and grow to equal grain size, at the locations in the slip bands. Depending on the local slide processes at the fracture point, it will subsequently start to spread [53], [54]. A stable phase of macro crack growth follows a stable phase of micro-crack propagation when smaller fissures join to form larger cracks. Finally, the remaining cross-section is ruptured due to the unstable fracture propagation and the static stress.
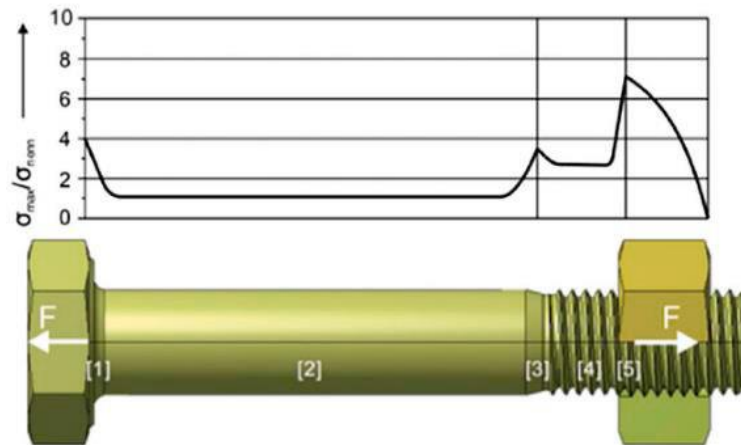
Figure 16. Fatigue failure locations in bolted assemblies [62]

Key factors that influence fatigue include the process of manufacturing and the bolt material [61]. Fatigue is also influenced by the stress concentrations and their location across the bolted assembly [63]. The factors that influence the fatigue strength of bolted connectors must be determined. The exact parameters which are pertinent to bolted connections in wind turbines are described in the section that follows.

According to Wiegand et al., the choice of material for bolting connections is based on the material's high strengths as well as its capacity to keep up a suitable level of toughness and ductility. In addition to enabling the preloads with a greater magnitude, is necessary to lower the imposed fatigue loading, this will also allow for a plastic redistribution of stresses in the thread. To exhibit the capabilities in the low alloy carbon steels, the bolts are necessary to be grade 8.9 or 10.9. The common extra alloying elements are included with chromium Cr, Nickel Ni, Molybdenum Mo, or Boron B [46].

Metals with high tensile strengths often enhance the metal's fatigue resistance. This effect, however, appears to be the opposite as the notch effect grows [64]. Additionally, it is reasonable to infer that a bolt's fatigue strength is unrelated to the strength of the bolt. The toughness characteristics of bolts are crucial in preventing early

cracking. Previous research has shown that at extremely low temperatures, brittle fractures of high-strength alloys and widths up to M64 are not evident [46]. Achmus and Schaumann have explained how the manufacturing process affects the microstructure of the bolt material, demonstrating how each of the different fatigue behaves. So, due to varying production methods and materials, it is rather very difficult to measure the effects of the bolts with different diameters [64], [65].

Furthermore, Eccles has shown that the bolt threads' surface finishes have an impact on the fatigue strength. He explained how threads that are being chopped and shaped tend to have shorter fatigue lives than threads that are rolled over smoother surfaces [66]. After, heat treatment bolt threads are rolled to create compressive stresses at the thread roots, which helps to minimize the crack initiation and, concurrently, greatly increases fatigue life. According to Eccles, when compared to ground threads, this manufacturing approach can greatly boost fatigue strength. Due to its lower cost, shot peening has taken place of this treatment. Additionally, larger-diameter bolts are being subjected to compressive pressures, which improve fatigue strength [66].

Achmus and Schaumann [64], [65] also found that residual stress at the boundary layer differed from the material of the bolt's core and was directly related to thickness. Matsunami was looking into how the pitch disparity and curvature radius of the threaded bottom affected fatigue strength. Additionally, he was attempting to create finite element models and an S-N curve. He discovered that the pitch difference has an impact on the initiation and spread of cracks [67]. Bolts are often hot-dip galvanized to prevent corrosion in offshore wind turbines (ORE). Schaumann and Eichstadt, noted that zinc-coated bolts frequently show a decrease in fatigue strength. They investigated the performance of M36 bolts that were hot-dip galvanized and coated in black at low, normal, and high temperatures [56].

When deciding whether to increase the size of bolts and reduce the number of bolts to achieve a better fatigue life in connections, there are several factors to consider. Uneven loading may result from increasing bolt size without increasing the number of bolts. Larger bolts and increased number of bolts, have a higher tensile strength and can have better connection and fatigue life [68].

2.2. Normative Method

Normative S-N curves are usually represented by the category of detail they possess, Ɣαc [61]. There are different fatigue strength curves for the direct strength ranges as shown in Figure 17.
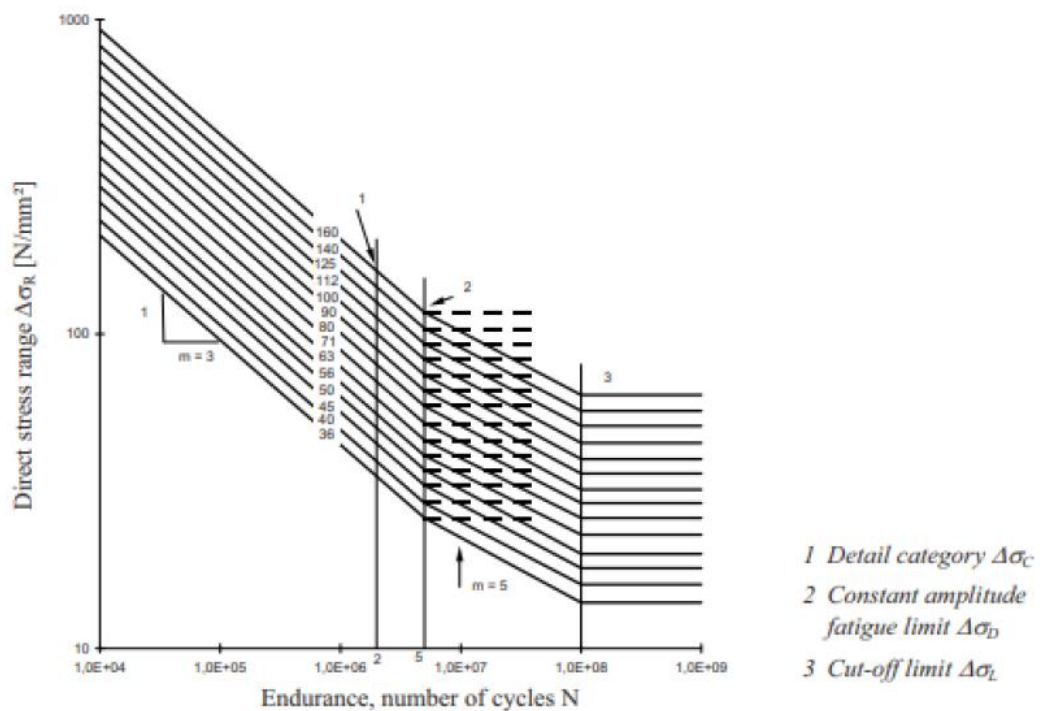
Figure 17. Direct stress ranges and fatigue strength curves [69]

From the above diagram, the modified strength of fatigue at $N_C = 2*10^6$ is calculated by these equations;

$$\Delta\sigma_{c,mod} = \frac{\Delta\sigma_c}{2} \, k_s \tag{4}$$

$$k_s = \left(\frac{30}{d}\right)^{0.25} \tag{5}$$

The reduction factor, K_s is found by the formula.

The formulae for calculating the limit constant amplitude fatigue are;

$$\Delta\sigma_D = \Delta\sigma_{c,mod} \left(\frac{N_c}{N_D}\right)^{\left(\frac{1}{m}\right)}, where \; m = 3 \tag{6}$$

With the constant amplitude fatigue known, the cut-off limit is obtained by this model;

$$\Delta\sigma_L = \Delta\sigma_D \left(\frac{N_D}{N_L}\right)^{\left(\frac{1}{m}\right)}, where \; m = 5 \tag{7}$$

The following expression can also be used to find points on the curve with a gradient of 1/3:

$$3 * log_{10} \, \Delta\sigma_R + log_{10}N_R = 3 * log_{10}\Delta\sigma_c + log_{10} 2 * 10^6 \tag{8}$$

The S-N curve's proximity and their values under specified formulae demonstrate that the results for the full diameter range of fatigue strength are extremely conservative [46]. The normative method provides an evaluation of a progression along a horizontal S-N curve with constant amplitude loading and load groupings whose

maximum values do not exceed stated the fatigue limit. The main purposes of the S-N curves in EC3 are to be implemented with Miner's linear damage accumulation and to verify service loads with varying amplitude. According to this reason, the development of the S-N curve after its knee point at $N = 5 \times 10^6$ is defined using Haibach's variation of Miner's rule. The fatigue strength threshold value after a horizontal progression with varied amplitude loading is set at $N = 10^8$ cycles.

2.3. Cycle Counting of Rainfall

Matsuishi and Endo [70] initially presented the rain flow measurement method in 1968. It was regarded as the initial widely acknowledged technique for recovering closed loading cycles. The method was given the name RF (Rainflow) because, when shifted vertically, it resembles a drop of rain falling down stress history. The cycle counting process moves from one local extreme to another starting at the beginning of stress or signal data. These regional data extremes could either be a peak or a valley.

According to the ASTM E1049 [71], which outlines the process step-by-step, the rain-flow counting approach is described in greater depth. ANSYS software was used for this project's rain-flow counting. Before determining partial damage, ANSYS divides the alternating and mean stresses into bins as part of its rain-flow counting process. The right number of bins is necessary for cycle counting to be accurate. The bin size for the history data loading type defines how many divisions should be being made for the cycle counting history. More specifically, the bin size defines how many divisions will be needed to create the rain-flow matrix.
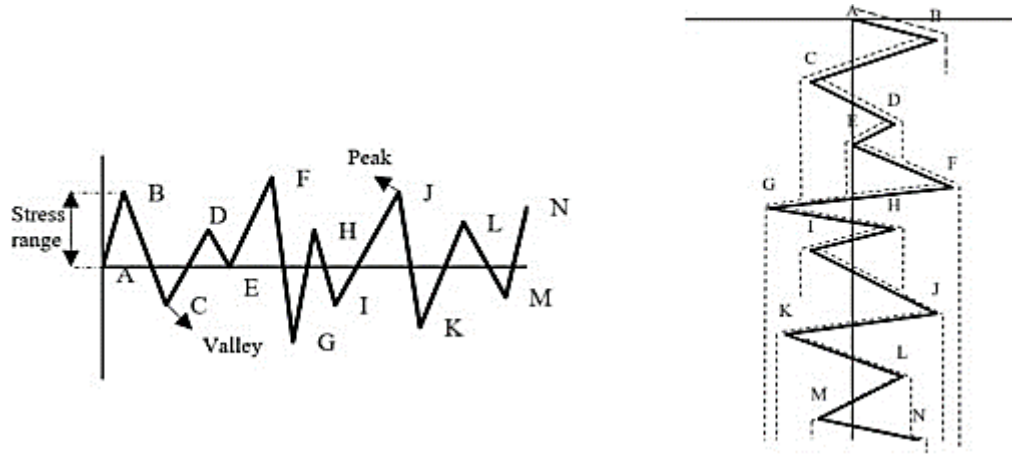
Figure 18. Illustration of random time series of stress including peaks and valleys and rain-flow counting approach for the signal [71] .

2.4. Average Stress Impact

Generally, the strength of fatigue in bolted assemblies declines with the rise in the average stress [69]. However, it is possible to control the impact of the mean stresses. The management of average stresses depends on the setup of the S-N curves [56]. The common action is that the knee point of the stress range is shifted along the S-N curve by a certain magnitude relative to the average stress targeted [72]. The average stress corrections can be represented by this models;

$$Soderberg: \frac{\sigma_{alternating}}{S_{endurance\ limit}} + \frac{\sigma_{mean}}{S_{yield\ strength}} = 1 \tag{9}$$

$$Goodman: \frac{\sigma_{alternating}}{S_{endurance\ limit}} + \frac{\sigma_{mean}}{S_{Ultimate\ strength}} = 1 \tag{10}$$

$$Gerber: \frac{\sigma_{alternating}}{S_{endurance\ limit}} + \left(\frac{\sigma_{mean}}{S_{yield\ strength}}\right)^2 = 1 \tag{11}$$

The various mean stress corrections are illustrated in Figure 19.
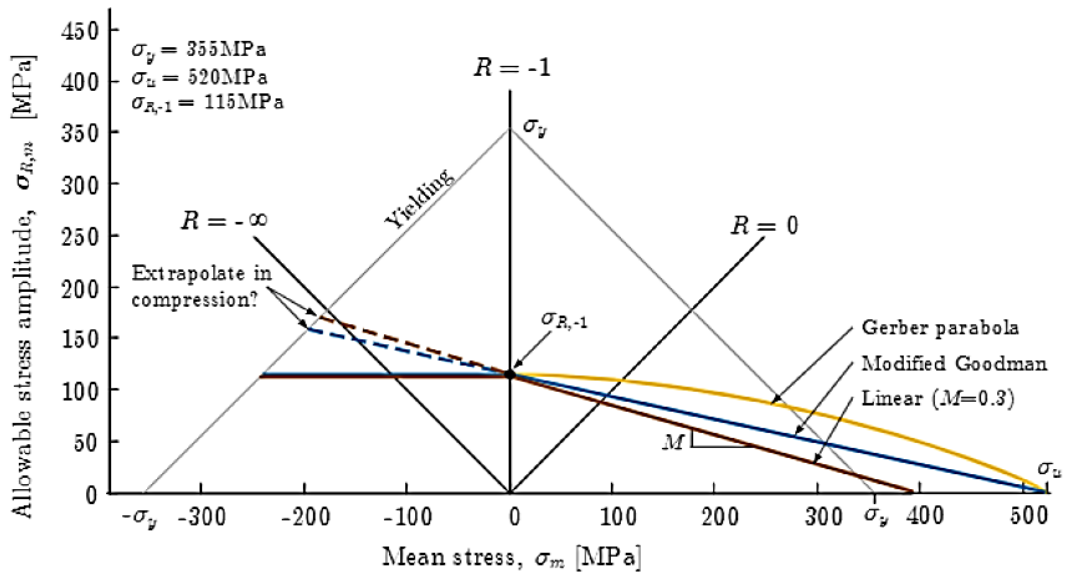
Figure 19. Various average stress corrections [73]

For the vast majority of available experimental data, the mean stress corrections often fall between those of Goodman and Gerber, with Soderberg proving to be more conservative. Goodman is a better choice for brittle materials, whereas Gerber is a better choice for ductile materials. Gerber means stress corrections accommodate for both positive and negative mean stresses. When taking into account negative means of stress, Wile Goodman and Soderberg do not feel constrained. This also prompts Goodman and Soderberg to be more careful since, even though compressive mean stress can retard the propagation of a fatigue fracture, doing so is typically more prudent than disregarding the negative mean.

2.5. Fatigue Evaluation Using Local Concepts

In fatigue design, besides the normative approach that uses nominal stress, there are several techniques that consider the notch root local loading conditions and displacements. By considering the local loading conditions and displacements at the notch root, it becomes possible to individually account for distinct influencing aspects

that are typically included in the design S-N curve of the structural member. Local concepts have the potential to assess specific aspects of the overall fatigue performance without the need for a time-consuming experimental test series with varying parameters. The utilization of these models requires a comprehension of the particular material properties, as they are based on the unique attributes of the base material. Moreover, the accuracy and reliability of the models' representations of actual physical behavior have an impact on local concepts. There are multiple techniques available for predicting the fatigue life between the initiation of a crack and failure, as well as the number of load cycles that can be sustained before the first fracture occurs. Eichstadt [46] offers comprehensive knowledge about the application of local concepts in fatigue testing of materials.

2.6. Beam Dyn and Elasto Dyn

Elasto-Dyn uses the Euler-Bernoulli beam theory to describe the blade as straight, isotropic beams with limited geometric non-linearities but simple flap-smart and edgewise bending deflections. (No torsion).

The FAST modularization architecture for wind turbine blade analysis comprises the BeamDyn structural dynamics module and the beam solver. BeamDyn.BeamDyn's capabilities were demonstrated and validated using numerical examples. The investigation began with a nonlinear beam deformation static benchmark problem. The results of BeamDynamics and the analytical solution accord quite well. In further precision convergence research, components of the convergence rate of Legendre were compared to regular quadratic finite elements. Expectedly, we observed exponentially convergent rates. Composite beams, as well as beams with

curved and twisted shapes, were studied. Comparisons with those from ANSYS and Dymore were made. Using two numerical examples, BeamDyn was assessed as either a FAST module or the FAST module coupling approach. BeamDyn's features may be summed up as follows:

- Static and dynamic geometric nonlinear beam difficulties/issues or problems with arbitrary magnitude displacements and rotations may be handled by BeamDyn using GEBT.

- When used in conjunction with something like a preprocessor like Pre-Comp or VABS, Beam-Dyn brings together all of the elastic coupling effects.

- Element of Legendre spectral finite like p-type element is used to discretize the spatial domain and resulting in exponential convergence rates for smooth solutions.

- Beam-Dyn is implemented in accordance with the FAST modularization framework's

2.7 Summary

This chapter has reviewed the literature related to this thesis. Then, the different aspects of wind turbine, fatigue, and stresses were reviewed. Finally, several software and codes had briefly explained.

CHAPTER 3: METHODOLOGY

This chapter will describe the methodology used in this thesis. Consequently, the wind simulation by TurbSim, Simulating forces created by the wind on the wind turbine, FEA Model, Material Selection, Geometry modeling, Contacts and frictions, Mesh Optimization, and Boundary Conditions and Loads to discuss the results.

3.1. Wind Simulation

The TurbSim Software, developed by the National Renewable Energy Laboratory (NREL), is a powerful simulation tool that enables the wind spectrum on wind turbines to be accurately calculated. The software takes into account the wind turbine's hub height, average wind speed, and turbulence to generate a realistic wind profile as shown in Figure 20.
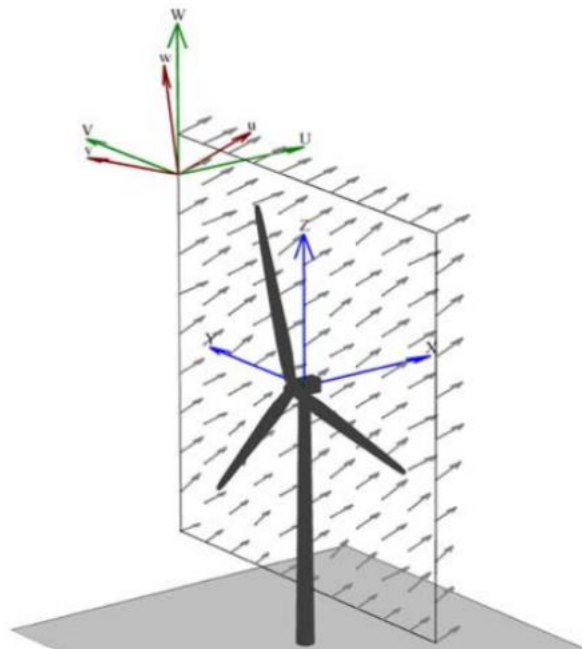
Figure 20. Illustration of a TurbSim wind field [74]

For a study conducted on the NREL 5MW wind turbine model, the simulation was computed at a hub height of 90m. To ensure a comprehensive analysis, four different wind speeds were chosen for the study: 5m/s, 10m/s, 15m/s, and 20m/s. These wind speeds were selected to represent the average wind speed in various countries. For instance, the average wind speed at a height of 90m in the Netherlands is 8.5m/s, while in Qatar, it is 5m/s. Table 1 provides a summary of all the design parameters used in the study [75].

In conclusion, the TurbSim software is a valuable tool for simulating the wind spectrum on wind turbines. The ability to take into account critical parameters such as hub height, average wind speed, and turbulence enables engineers to make accurate predictions about the performance of wind turbines under different operating conditions. The results of these simulations can be used to optimize the design of wind turbines and improve their overall efficiency.

Table 1. Wind field parameters and meteorological boundary conditions

Wind field parameter	Value	Unit
Vertical grid-point matrix dimension	31	m
Horizontal grid-point matrix dimension	31	m
Grid height	145	m
Grid width	145	m
Meteorological Boundary condition	Value	Unit
Hub height	90	m
Spectral model	IEC Kaimal	-
Turbulence model	IEC Kaimal	-
Reference height	90	m
Power law exponent	0.200	-
Surface roughness length	0.030	m
Average wind speed	5, 10, 15, 20	m/s

The main objective of this section is to provide a concise explanation of the TurbSim code and its functions. The source code is open-source and was utilized in the dissertation work. TurbSim begins by reading an input file containing user-specified parameters, including the IECKaimal turbulence model, which follows the IEC standard. It then determines the correct sigma for each component based on the specified spectral and turbulence model.

TurbSim does a few things to calculate wind speeds across a grid. It starts by reading a file and using the information to generate some random numbers. It then uses those numbers to calculate some other values that help determine wind speeds. After that, it checks if the wind speeds meet certain requirements, and if not, it adjusts a setting. Finally, it calculates the average wind speed and turbulence for the entire grid and compares it to what was expected. Additionally, the flow chart gives an overview of the TurbSim simulation method. This code is a valuable tool in predicting the performance of wind turbines under different operating conditions, and it is widely used in the field of renewable energy research. The ability to specify user-defined parameters and follow international standards ensures that engineers and researchers can achieve accurate and reliable results. Figure 21 shows an overview of TurbSim simulation method.

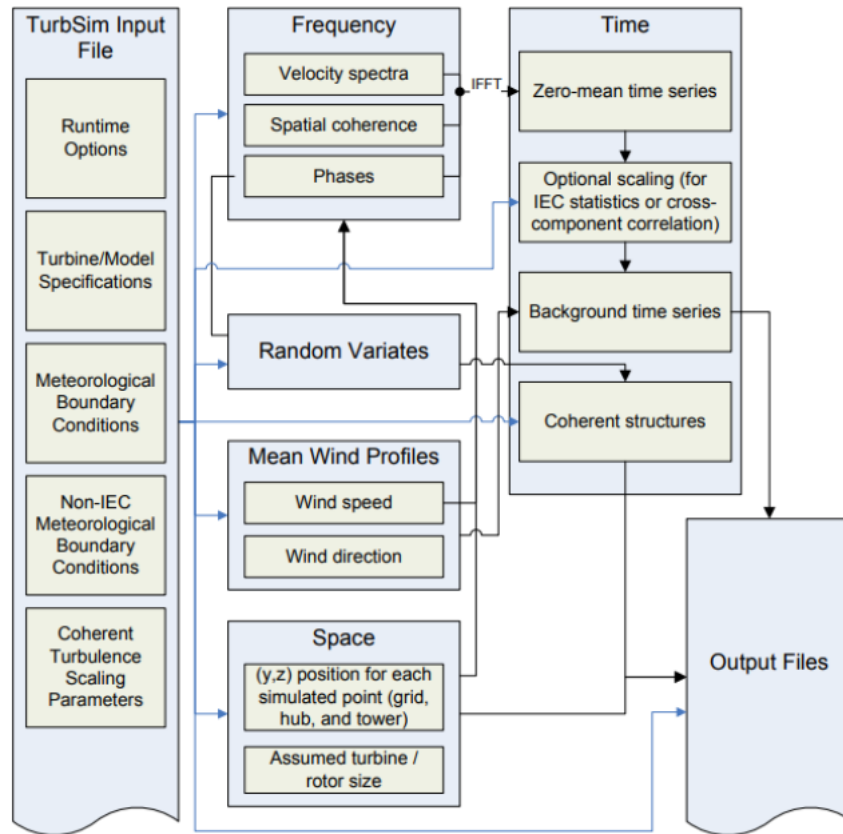Figure 21. Overview of TurbSim simulation method: blue lines - input-file parameters, black lines - internal variables/processes [76]

As discussed above, the results obtained from Turbsim will serve as input for the FAST program. Figure 22 is a sample of the wind spectrum generated by Turbsim with an average wind speed of 10 m/s.
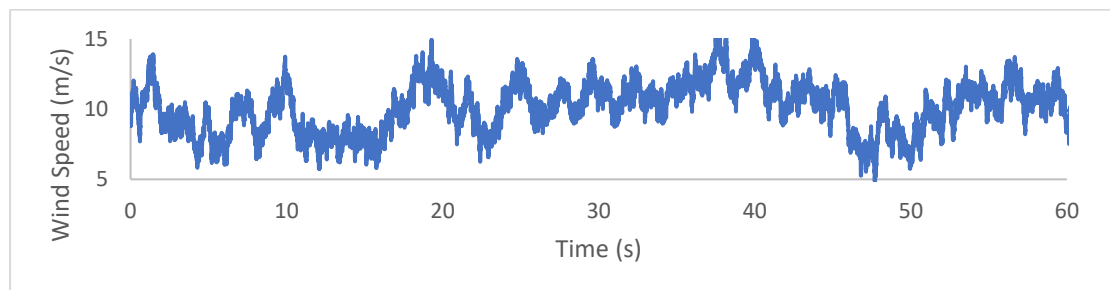

Figure 22. Wind Spectrum Result from Turbsim at an average wind speed of 10 m/s

3.2. Simulating Forces Created by Wind on The Wind Turbine

The FAST code is a widely used software tool in the field of wind energy. It is a powerful simulation tool that can predict the behavior of wind turbines under different conditions. One of the key features of FAST is its ability to accurately calculate the fatigue loads on wind turbine components.

In FAST, fatigue is computed in terms of loads rather than stresses. This is because it is the loads that cause fatigue damage to the components, and not the stresses themselves. By accurately calculating the loads, FAST can predict the fatigue life of different components, and help engineers design wind turbines that are reliable and durable.

The FAST code is based on a combined modal and multi-body structural formulation. This means that it uses both modal analysis and multi-body dynamics to model the wind turbine system. This allows for accurate simulations of the complex interactions between different components of the turbine.

At each time step, FAST calculates the aerodynamic, gravitational, and aeroelastic forces acting on the structure. These forces are used to solve the nonlinear equations of motion for the different displacements and states of the structural components. This enables FAST to accurately predict the dynamic behavior of the wind turbine system under different conditions.

FAST has the flexibility to translate the modal structural model into multi-body models of wind turbine models. This allows engineers to choose the most appropriate modeling approach for their specific application. Additionally, FAST allows the extraction of a linearized representation of the model for other purposes. This means that engineers can use the model to design control systems and other applications that require a linear model.

In summary, the FAST code is a powerful simulation tool that can accurately predict the dynamic behavior of wind turbines under different conditions. Its ability to accurately calculate fatigue loads and its flexible modeling approach makes it a valuable tool for wind turbine design and optimization. FAST's work methodology for fixed-bottom systems is depicted in Figure 23
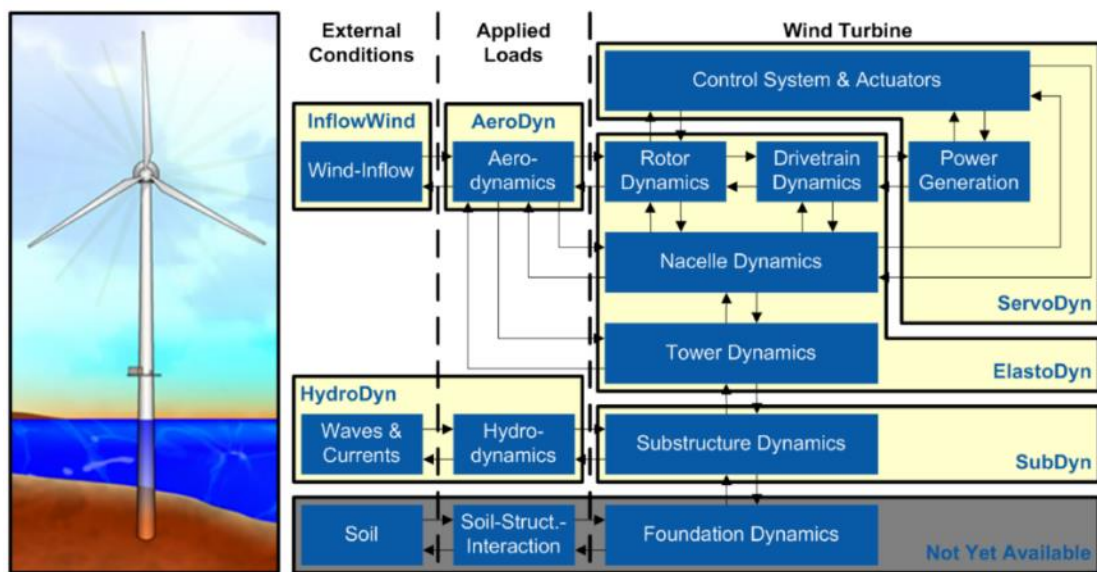
Figure 23. Work methodology of FAST for fixed-bottom systems [77].

The purpose of this mathematical model is to illustrate all static and dynamic loads that the wind turbine may experience at any point based on the user's assigned data. The software includes multiple tests for various wind turbine models. After studying all the test cases, Test 18 was chosen for this thesis. Test 18 is a 3-bladed onshore 5MW wind turbine model with a rotor diameter of 126m. This test considers tower flow and drags in addition to wind spectrum and turbulence.

The mathematical model includes all geometrical and material properties of the wind turbine, as shown in Table 2. Structural steel is used for the wind structure, and the density of the structural steel in the FAST software is 8500 kg/m3, which includes

the weight of the paint, bolts, and nuts in the simulation. This level of detail in the model allows for accurate predictions of the structural behavior and performance of the wind turbine under different loads and conditions.

Table 2. NREL 5MW wind turbine material and geometric specifications

Property	Value	Unit
Tower height	87.6	m
Top tower outer diameter	3.87	m
Top tower shell thickness	0.0247	m
Base tower outer diameter	6	m
Base tower shell thickness	0.0351	m
Density	8500	kg/m^3
Young's modulus	210	GPa
Shear modulus	80.8	GPa

The table above indicates that the wind turbine tower is a truncated conical shape, with a diameter that decreases from 6 m at the base to 3.87 m at the top. The dimension of the tower truncated conical shape are represented in Table 3

Table 3. Tower truncated conical shape dimensions

Tower Elevation (m)	Tower Diameter (m)
0	6
8.526	5.787
17.053	5.574
25.579	5.361
34.105	5.148
42.633	4.935
51.158	4.722
59.685	4.509
68.211	4.296
76.738	4.083
85.268	3.870
87.600	3.870

The objective of this thesis is to investigate the fatigue life of flanged bolt connections located in the lower third of the tower. However, to study the precise location of the tower, increasing the number of tower nodes is necessary, which can be time-consuming and expensive. Therefore, the nodes of the tower were kept as default to minimize simulation costs.
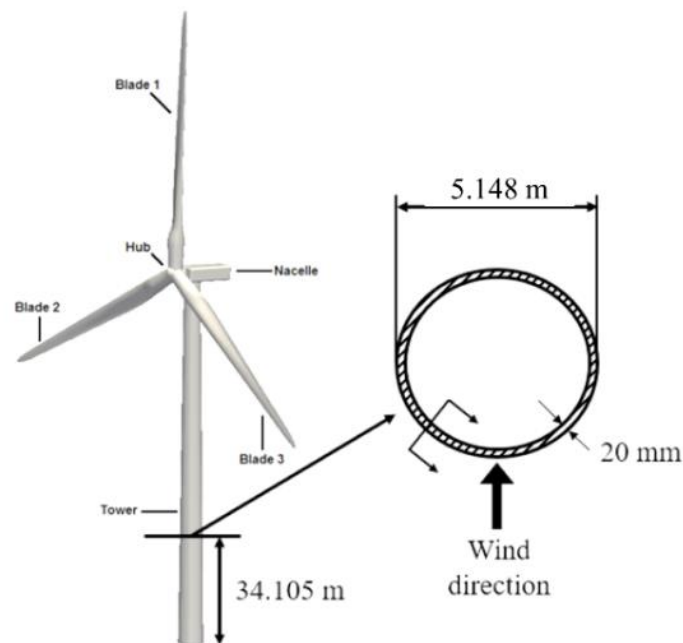
Figure 24. Bolted flange location

FAST software provides various functions to simulate the parameters that affect wind turbine performance. These functions can be modified by the user based on their case study. Some of these functions are:

- ElastoDyn: simulates the environmental conditions, tower properties, kinematics, turbine configuration, drivetrain properties, blade properties, and degrees of freedom.

- BeamDyn: simulates the specifications for the pitch actuator, geometry, mesh, and material.

- AeroDyn: simulates unsteady airfoil aerodynamics, additional environmental conditions, blade-element design, and rotor/blade configuration.
- InflowWind: contains the wind spectrum data generated by TurbSim.

Once these functions are modified, the user can run the software to obtain the forces applied to the structure. It should be noted that FAST uses a different coordinate system, so users must pay attention while transferring the results. These results can be used as input data in the fatigue analysis.

Once the wind spectrum generated by Turbsim is implemented in FAST, the program will calculate the axial force and bending moment exerted on the wind turbine. Figure 25 and Figure 26 demonstrate the axial force and bending moment calculated by FAST at an average wind speed of 10 m/s.
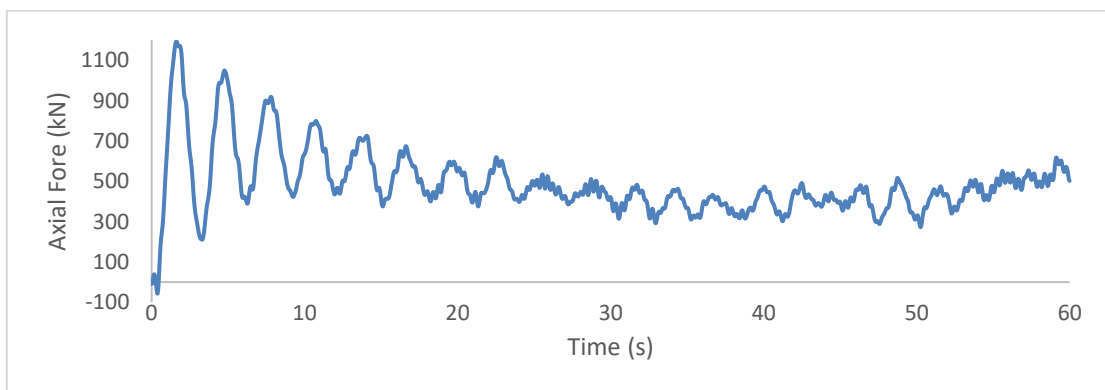
Figure 25. Axial Force applied on the wind turbine tower by 10m/s wind Spectrum.
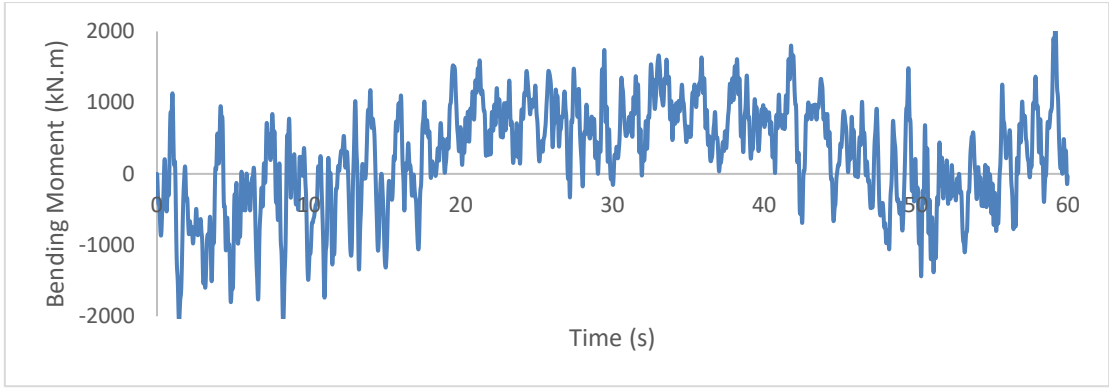
Figure 26. Bending Moment applied on the wind turbine tower by 10m/s wind Spectrum.

The loads will be combined using the following equations to determine the resulting stress inside the wind turbine tower, which will be the tensile stress.

$$T_o = \frac{F_{axial}}{A_{tower}} + \frac{M_{bending}}{S_{tower}} \tag{12}$$

F_{axial} and $M_{bending}$ represent the axial force and bending moment at the specified cross-sectional location of the wind turbine tower. The tower's cross-sectional area A_{tower} and section modulus S_{tower} will be calculated by

$$A_{tower} = \pi(R^2 - r^2) \tag{13}$$

$$S_{tower} = \pi \frac{D^4 - d^4}{32D} \tag{14}$$

The outer radius of the tower's cross-sectional area is represented by R, and the inner radius is represented by r. Meanwhile, the outer diameter of the tower is represented by D, and the inner diameter is represented by d. The resulting cross-

39

sectional areas are shown in Table 4.

Table 4. Cross-sectional areas

Parameters	Value
A_{tower}	0.322 m^2
S_{tower}	0.206 m^3

The traction stress results, calculated using the equations mentioned above, are shown in Figure 27 at the flange location inside the wind turbine tower. These outcomes will be employed in the simulation to examine the fatigue life of the bolted flange connection.
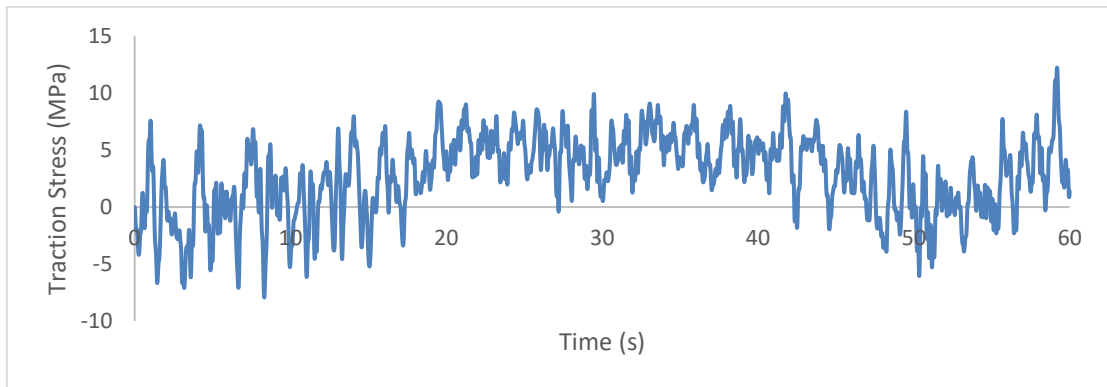
Figure 27. Traction Stress applied on the flange location.

3.3. FEA Model

The fatigue analysis in this thesis will be conducted using ANSYS software, which is a powerful tool for structural analysis. In order to accurately simulate the fatigue life of the flanged bolt connection at the lower third of the wind turbine tower, several design steps are required.

The number of bolts in bolted flange connections is very important when designing bolted connections to consider the number of bolts used in it.

Material selection is a crucial aspect that needs to be considered carefully. The

material properties such as yield strength, ultimate strength, and Young's modulus should be defined accurately to reflect the actual properties of the material used in the wind turbine tower.

Geometry modeling needs to be performed to create a detailed 3D model of the flanged bolt connection. This involves defining the dimensions, shapes, and orientations of the components in the connection. Also, Contact identification is necessary to accurately simulate the interaction between the bolt and the flange. This step involves defining the contact regions, the contact type, and the friction coefficients.

Meshing optimization is important to ensure accurate simulation results. The mesh should be refined in critical areas and coarser in areas where stress concentration is not expected. Boundary Conditions and Loads need to be defined to simulate the actual loading conditions of the wind turbine tower. This includes defining the boundary conditions such as fixed supports, applying loads such as wind loads, and defining the load history. Also Understanding the fatigue tool will lead to more representing fatigue life results.

By following these design steps, an accurate simulation of the fatigue life of the flanged bolt connection can be achieved, which is essential for ensuring the reliability and safety of the wind turbine tower.

3.3.1. Number of bolts

In order to ensure a robust connection, it is recommended that the flange area be covered by bolts as extensively as possible. The present study will therefore take into account the number of bolts used in the bolted flange. The number of bolts will vary depending on the bolt size and the maximum number of bolts that can be accommodated for a given size will be considered. Specifically, the number of bolts

will be evaluated from 120 bolts up to the maximum allowable for the specific size. It is important to note that the maximum number of bolts that can be utilized will be impacted by the size of the bolts. For example, the M48 bolt cannot reach 200 bolts since the bolt heads will collide with each other.

3.3.2. Material Selection

Based on the NREL 5MW wind turbine model, the tower is constructed using structural steel. In contrast, high-carbon steel is commonly used as the material for bolts. It is worth noting that high-carbon steel has a better fatigue life compared to structural steel. Furthermore, the microstructure of high-carbon steel is more uniform than that of structural steel, which further enhances its fatigue life. It is crucial to consider the material properties and their impact on the fatigue life of the components in the wind turbine to ensure the safe and reliable operation of the turbine. [78][79].

However, for the purpose of studying the impact of bolt number and size, both the tower and bolts in this thesis will be considered structural steel. Figure 28, Figure 29 and Figure 30 illustrate the material specifications of the structural steel.

	A	B	C	D	E
1	Property	Value	Unit	⊗	🖅
2	📝 Material Field Variables	🔳 Table			
3	📝 Density	7850	kg m^-3 ▾	☐	☐
4	⊟ 📝 Isotropic Secant Coefficient of Thermal Expansion			☐	
5	📝 Coefficient of Thermal Expansion	1.2E-05	C^-1 ▾		☐
6	⊟ 📝 Isotropic Elasticity			☐	
7	Derive from	Young's Modulu... ▾			
8	Young's Modulus	2E+11	Pa ▾		☐
9	Poisson's Ratio	0.3			☐
10	Bulk Modulus	1.6667E+11	Pa		☐
11	Shear Modulus	7.6923E+10	Pa		☐
12	⊞ 📝 Strain-Life Parameters			☐	
20	⊟ 📝 S-N Curve	🔳 Tabular		☐	
21	Interpolation	Log-Log ▾			
22	Scale	1			☐
23	Offset	0	Pa		☐
24	📝 Tensile Yield Strength	2.5E+08	Pa ▾	☐	☐
25	📝 Compressive Yield Strength	2.5E+08	Pa ▾	☐	☐
26	📝 Tensile Ultimate Strength	4.6E+08	Pa ▾	☐	☐
27	📝 Compressive Ultimate Strength	0	Pa ▾	☐	☐
28	📝 Isotropic Thermal Conductivity	60.5	W m^-1 C^-1 ▾	☐	☐
29	📝 Specific Heat, C_9	434	J kg^-1 C^-1 ▾	☐	☐
30	📝 Isotropic Relative Permeability	10000		☐	☐
31	📝 Isotropic Resistivity	1.7E-07	ohm m ▾	☐	☐

Figure 28. Structural steel specifications

	B	C
1	Cycles	Alternating Stress (Pa)
2	10	3.999E+09
3	20	2.827E+09
4	50	1.896E+09
5	100	1.413E+09
6	200	1.069E+09
7	2000	4.41E+08
8	10000	2.62E+08
9	20000	2.14E+08
10	1E+05	1.38E+08
11	2E+05	1.14E+08
12	1E+06	8.62E+07

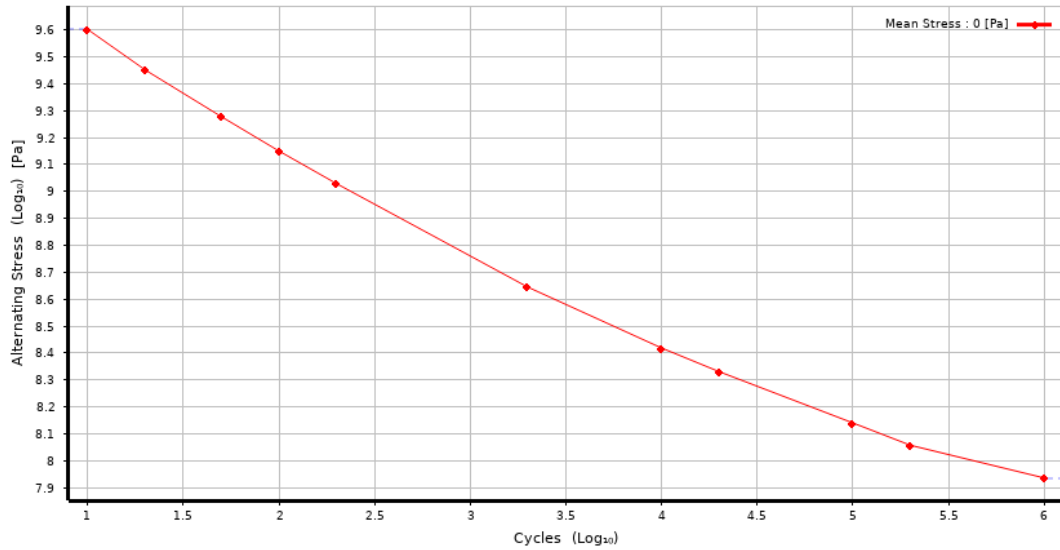Figure 29. S-N Curve Data for structural steel

Figure 30. S-N log-log curve for structural steel

3.3.3. Geometry Modeling

The design for this study was created using the ANSYS Workbench design module, with all parameters being parametrized for ease of modification. The flange design was based on similar applications as found in [80]. and the schematic for the design is shown in Figure 31.
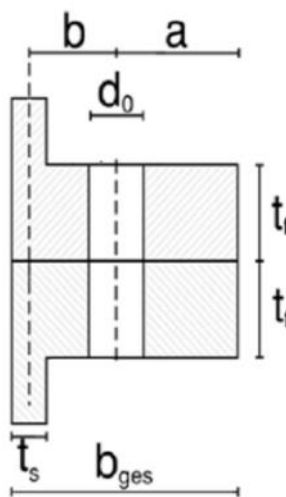

Figure 31. Schematic of the flange design

The diameter of the flange will be determined based on the specific location of the wind turbine tower.

44

Table 5. Flange dimensions

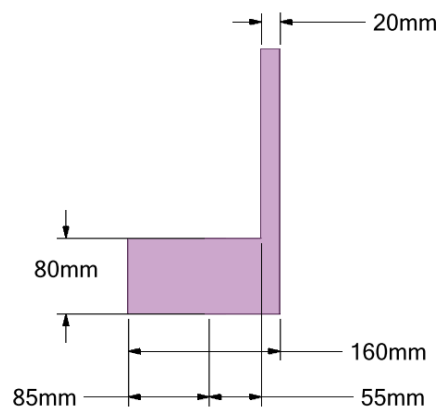| Description	Symbol	Value (mm)
Shell thickness	t_s	20
Flange thickness	t_f	80
Flange width	b_{ges}	160
Dist. bolt center to flange edge	a	85
Dist. bolt center to shell center	b	65

Figure 32. Flange dimensions in design modular

In this thesis, three bolt sizes will be studied, namely M36, M42, and M48. The dimensions of these bolts are shown in the Figures below and they were drawn according to ASME standards.
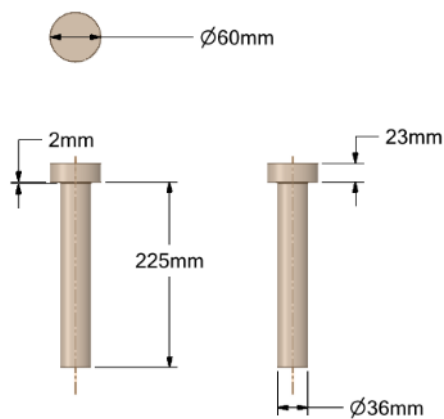

Figure 33. M36 Bolt dimensions
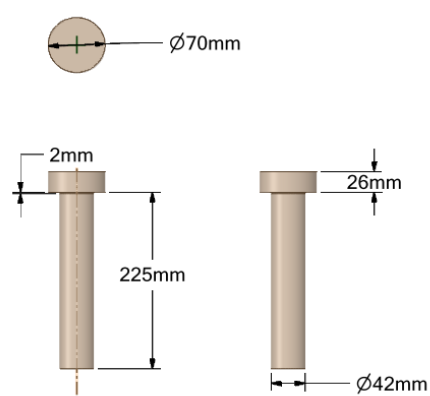
Figure 34. M42 Bolt dimensions
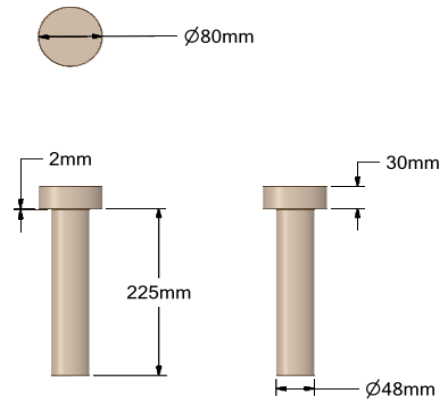
Figure 35. M48 Bolt dimensions
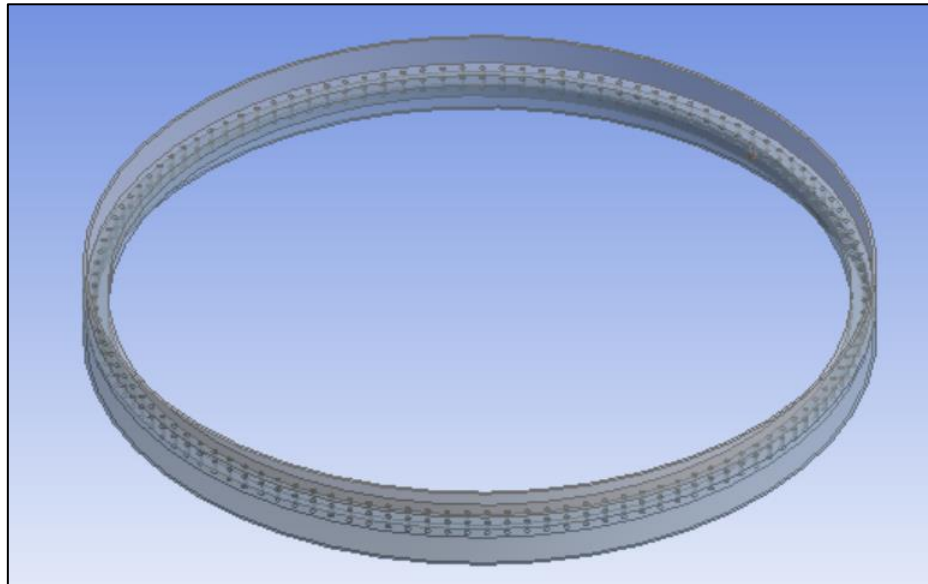
Figure 36. Flange full design

In order to prevent an enormous amount of time and number of elements required for simulation, the software did not include the full model as shown in Figure 36 . Since the flange design is symmetrical, the loads affect all bolts equally. Therefore, the simulation will be performed on one part of the flange as shown in Figure 37. The width of this part was designed to utilize symmetry, by taking half the distance between the bolts in both directions into account. Therefore, the width will vary depending on the number and size of bolts used in the flange.
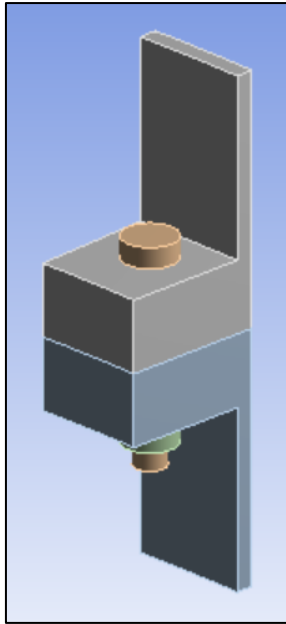
Figure 37. One part of the flange

3.3.4. Contacts and Frictions

The contact between the bolt and the flange, and between the nut and the flange was modeled as frictional contacts with a coefficient of friction of 0.2. The commonly used value of the friction coefficient between structural steel surfaces in engineering simulations is 0.2. Research by Sahin and Kilic has shown that this value can vary between 0.15 and 0.3, depending on factors such as surface roughness [81].

The contact between the nut and the bolt shank was modeled as a bonded contact to accurately simulate the effect of threads in real life. The contacted surfaces are illustrated in the exploded view of Figure 38, where the red and blue surfaces represent the contact areas.

Figure 38. Contact areas in the model

3.3.5. Mesh Optimization

Meshing plays a crucial role in the accuracy of the simulation results. A finer mesh generally provides more accurate results, but it is not always practical to use the smallest possible mesh size due to the significant increase in the number of elements, simulation cost, and run time. A balance between the mesh size and the accur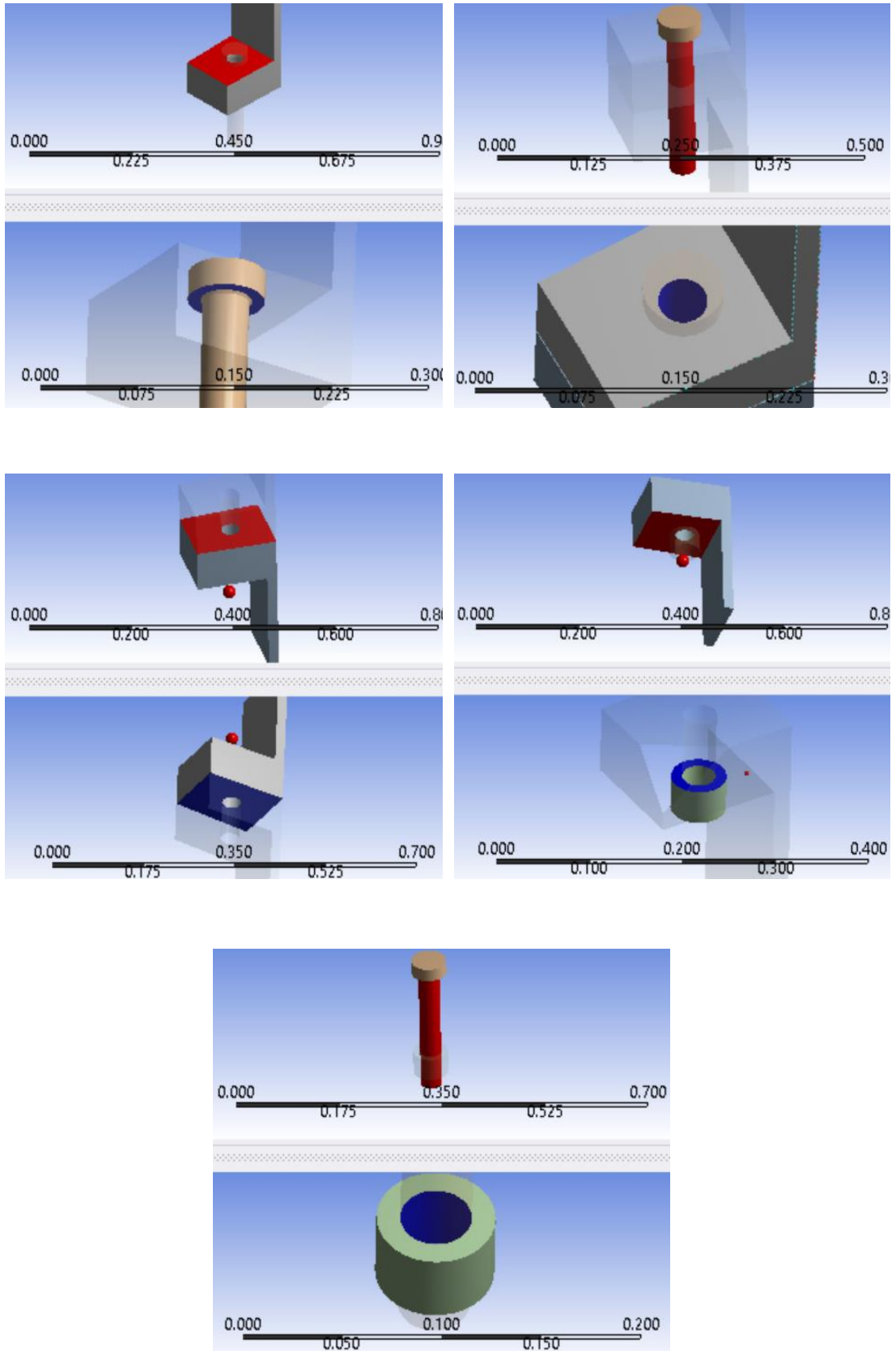acy of the results is essential. Therefore, to obtain the optimum mesh size that provides the best results while also saving costs and time, several mesh convergence studies were performed.
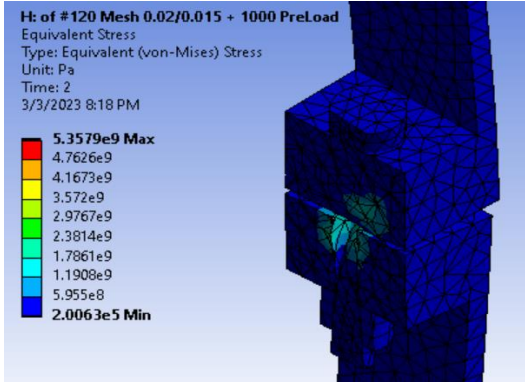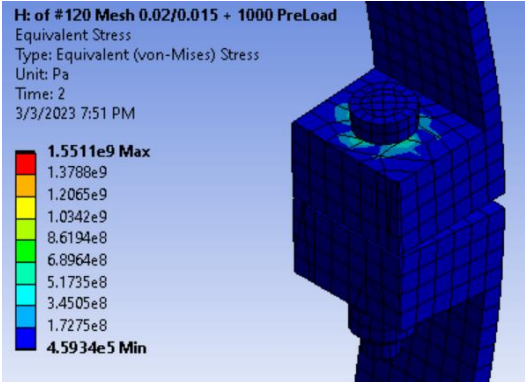
The accuracy of simulation results is strongly influenced by the meshing technique used. However, decreasing the element size of the mesh can result in a massive increase in the number of elements, thereby increasing the simulation cost and run time. Therefore, the meshing process was optimized to achieve the best results while saving time and cost. The first step in the meshing process was to determine whether the elements' size of the flange structure affected the results. This was achieved by conducting a test that kept the bolt structure's mesh elements constant while changing the flange structure's mesh size. The results indicated that the elements' size of the flange structure affected the results and required modification in the optimization of the mesh optimization study.

For a uniform geometry, the use of multizone mesh elements may result in more accurate and realistic results. According to research by Zhang et al, multizone meshes can provide better accuracy than traditional single-zone meshes in certain situations, such as when dealing with complex geometries or areas of high-stress concentration. This is because multizone meshes can better capture the variations in stress and strain across different regions of the model [82].

However, it is important to note that the choice of mesh element type should also consider other factors such as computational efficiency, as multizone meshes can be more computationally expensive. Ultimately, the choice of mesh element type should be carefully evaluated based on the specific simulation requirements and a balance between accuracy and computational cost.

To optimize the mesh size, sixteen tests were conducted using two different methods: auto-free mesh and multizone mesh. Eight cases were studied for each method, and the goal of these tests was to check the convergence of the results. Based on the literature review in chapter 2, bolts were expected to fail due to fatigue. Therefore, the bolt mesh was designed to be smaller than the flange mesh to obtain more representative results. The sixteen tests' parameters and results are presented in Table 6.

Table 6. Mesh results for all tests

Test 1. Stress Results (MPa)	
Flange elements size = 0.02 and Bolt elements size = 0.015	
a) Auto-Free Mesh	b) Multizone Mesh

Test 2. Stress Results (MPa)

Flange elements size = 0.015 and Bolt elements size = 0.0125

c) Auto-Free Mesh	d) Multizone Mesh

Test 3. Stress Results (MPa)

Flange elements size = 0.0125 and Bolt elements size = 0.01

e) Auto-Free Mesh	f) Multizone Mesh

Test 4. Stress Results (MPa)

Flange elements size = 0.01 and Bolt elements size = 0.0075
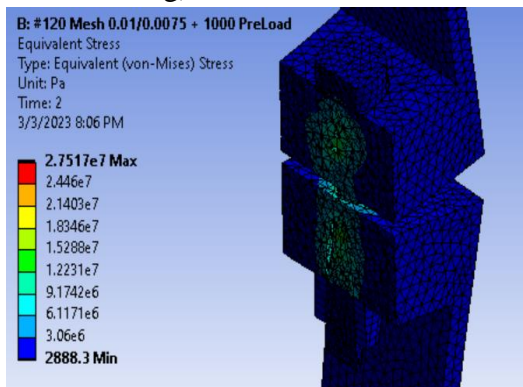
g) Auto-Free Mesh	h) Multizone Mesh
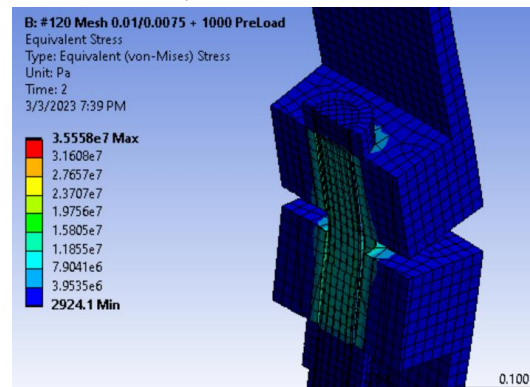
Test 5. Stress Results (MPa)

Flange elements size = 0.0075 and Bolt elements size = 0.005
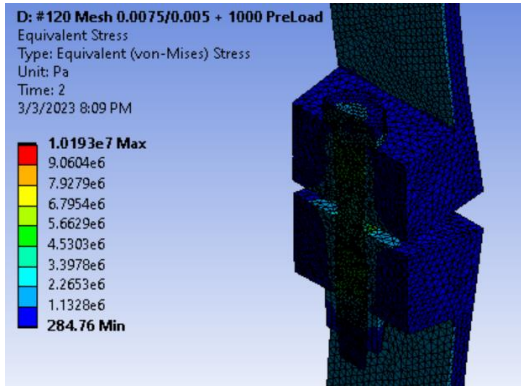
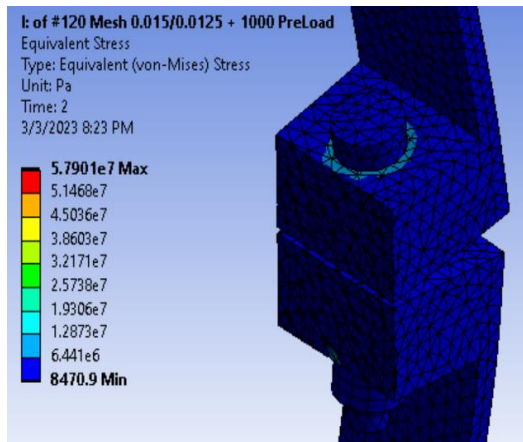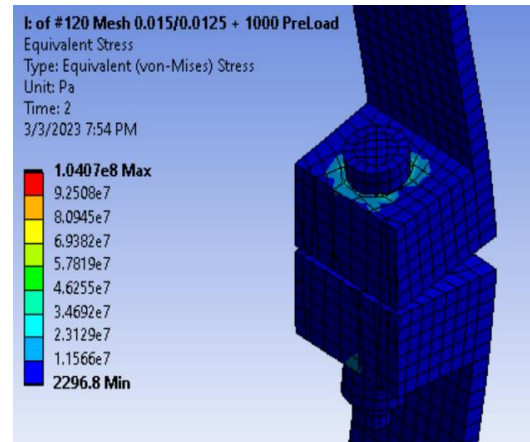| i) Auto-Free Mesh	j) Multizone Mesh
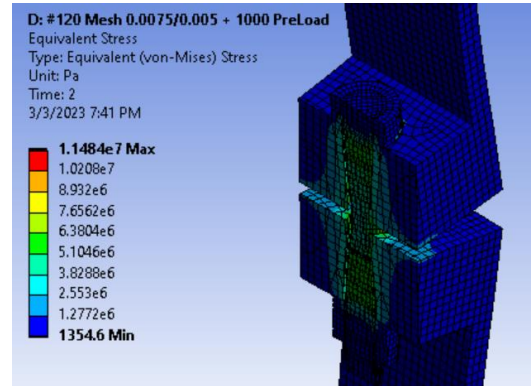
Test 6. Stress Results (MPa)

Flange elements size = 0.005 and Bolt elements size = 0.0025
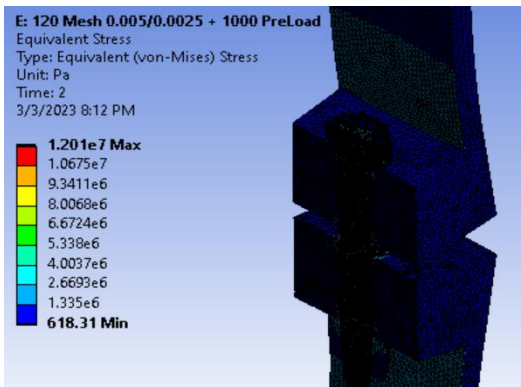
k) Auto-Free Mesh	l) Multizone Mesh
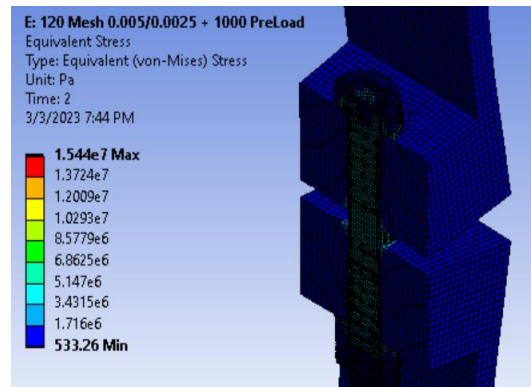
Test 7. Stress Results (MPa)

Flange elements size = 0.0035 and Bolt elements size = 0.0025

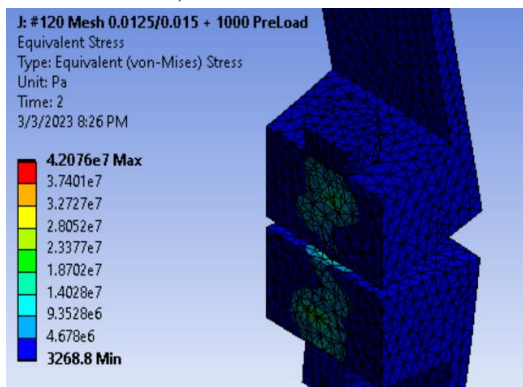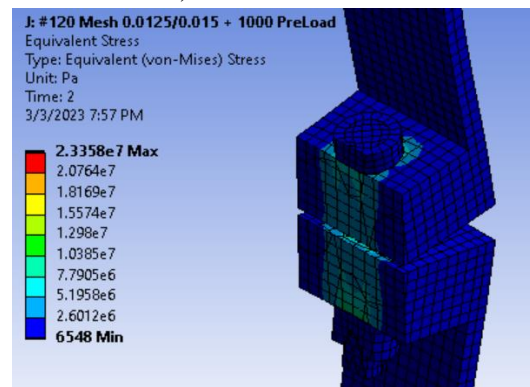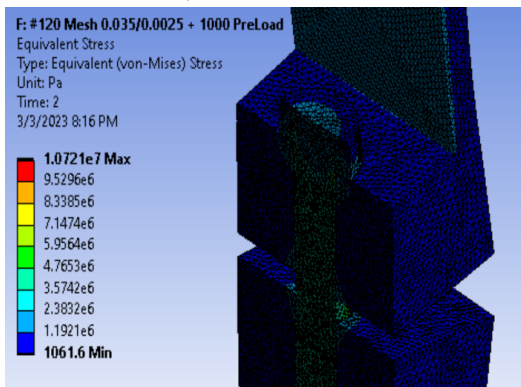| m) Auto-Free Mesh	n) Multizone Mesh
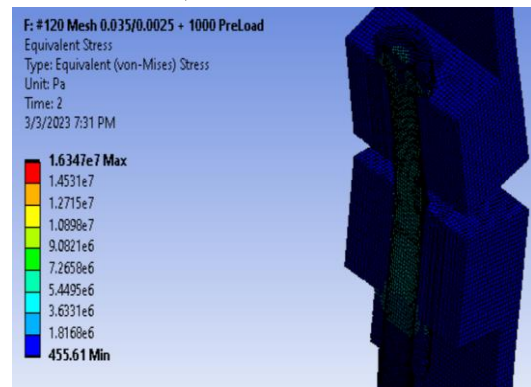
Test 8. Stress Results (MPa)	
Flange elements size = 0.0035 and Bolt elements size = 0.002	
o) Auto-Free Mesh	p) Multizone Mesh
N/A	
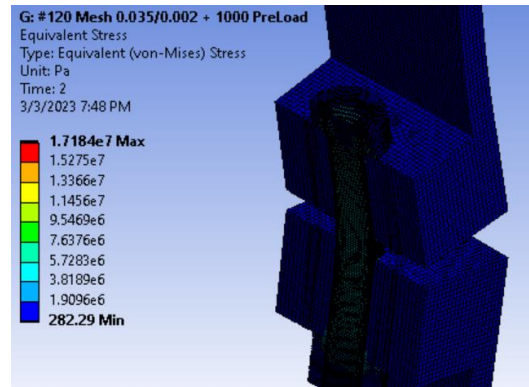
The mesh element sizes were tested for both the auto mesh and multizone mesh, with a range starting from a flange element size of 0.02 m and a bolt element size of 0.015 m, and gradually decreasing to a flange element size of 0.0035 m, and a bolt element size of 0.002 m.

Table 7. Test parameters and Results

Test #	Size of Flange elements (m)	Size of Bolt elements (m)	Stress Results (MPa)	
			Auto Free Mesh	Multizone Mesh
1	0.02	0.015	5357	1551.1
2	0.015	0.0125	57.901	10.407
3	0.0125	0.01	42.076	23.358
4	0.01	0.0075	27.517	35.558
5	0.0075	0.005	10.193	11.484
6	0.005	0.0025	12.01	15.44
7	0.0035	0.0025	10.721	16.347
8	0.0035	0.002	N/A	17.184
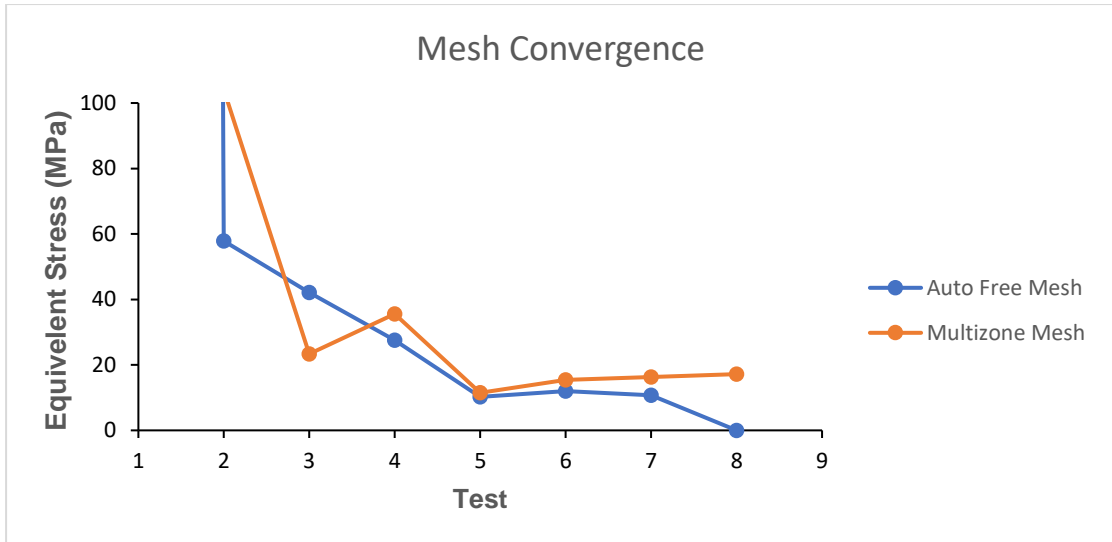
Figure 39. Mesh convergence behavior.

It is clearly shown in Figure 39 that the multizone mesh showed better convergence behavior corresponding to these sizes. Moreover, the auto mesh started showing errors when the mesh size decreased. Furthermore, the skewness and mesh quality of the multizone mesh is superior to the auto-free mesh. Thus, the study will be computed using the multizone and to save the simulation cost, the elements mesh parameters will be taken from Test 7 since it is in the convergence range and has fewer elements and runtime compared to Test 8. Figure 40 shows the designed mesh and Table 8 shows the mesh quality and skewness of Test 7 parameters.
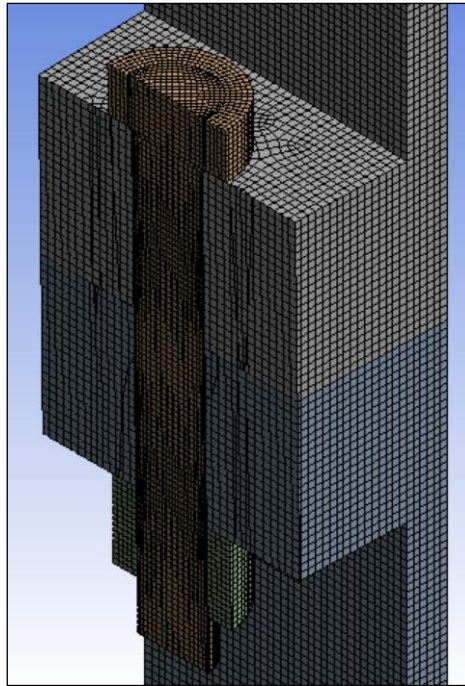
Figure 40. Designed mesh

Table 8. Mesh quality and skewness of Test 7

Parameter	Average
Mesh Quality	0.95606
Skewness	0.074348

This means that the mesh is of high quality and there are no distortions or issues that could impact the accuracy of the simulation results.

3.3.6. Boundary Conditions and Loads

The bottom face of the structure is fixed support while the sides are frictionless supports. The sides were given frictionless support to simulate that the design is a small portion of the flange and these sides are bonded to the flange where there is no friction. This constrains translation in a specified direction while allowing rotation around all three axes, assuming zero friction between the support and the body, and enabling free

movement perpendicular to the constraint direction. A traction stress load of 1 MPa is applied to the top of the upper flange, Figure 42 shows all the loads and boundary conditions applied to the design. which serves as a multiplier coefficient to the fatigue data obtained from FAST. To ensure consistency, the computed fatigue data is also expressed in MPa. In addition, a preload was applied to the bolt to make the simulation more realistic, although the focus of this thesis is not on the effect of preload. The application of a preload value of 1 kN is intended to highlight to future researchers and designers the importance of considering preload when designing the full flange. then it was locked. The analysis was conducted in two steps. In the first step, a preload was applied and locked as shown in Figure 41. To prevent it from being repeated in each cycle during the application of the fatigue data. In the second step, the pressure was applied.

Steps	Define By	Preload [N]	Preadjustment [m]	Increment [m]
1 1.	Load	1000.	N/A	N/A
2 2.	Lock	N/A	N/A	N/A
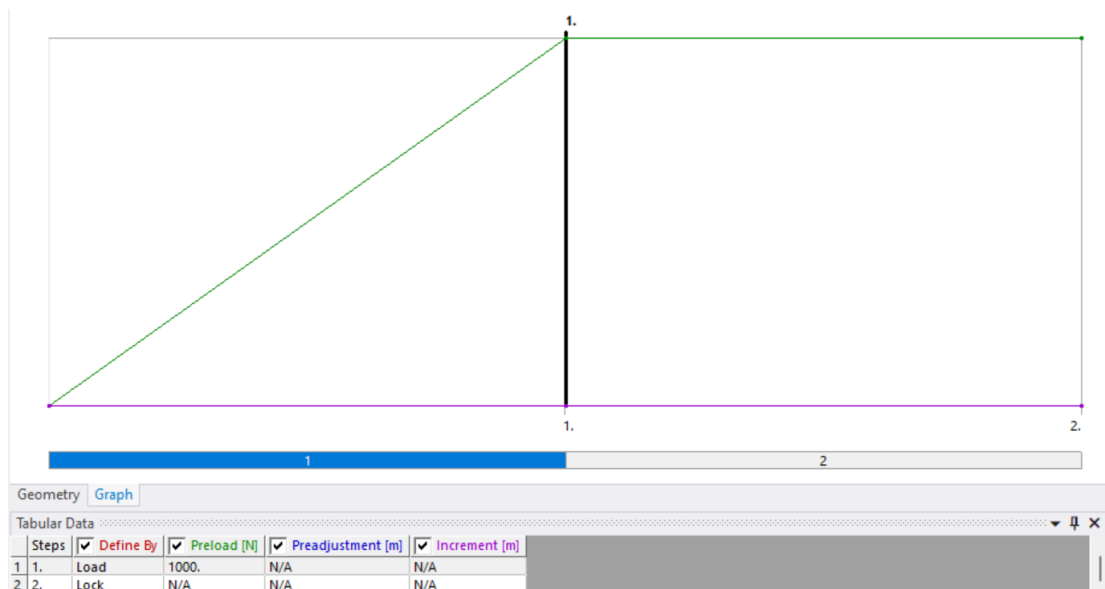
Figure 41. locking the pre-load after the first step.
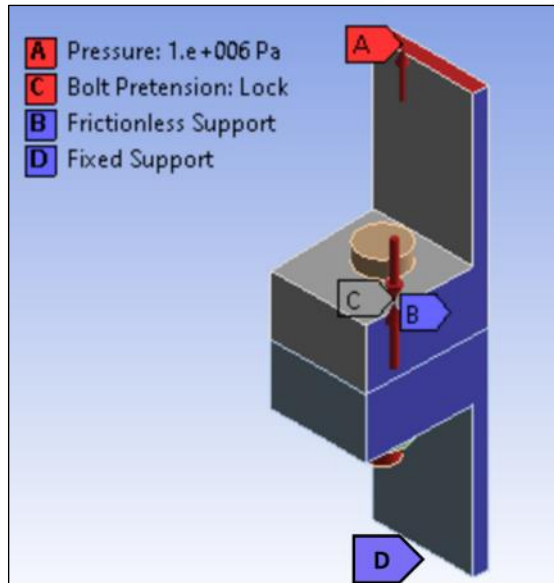
Figure 42. Loads and boundary conditions applied on the flange

3.3.7. Fatigue Tool

The ANSYS fatigue tool is a software that can assess and predict the fatigue life of a structure undergoing cyclic loading. It employs different models and techniques to determine the amount of damage that the structure will encounter and how long it will remain functional based on the applied load and material properties.

To utilize the ANSYS fatigue tool, the user is required to provide details regarding the properties of the structure and the loading conditions it is subjected to. The tool then applies these parameters to a computer model, calculating the response of the structure under repeated loading. It then estimates the remaining life expectancy of the structure using different models for various types of damage.

The ANSYS fatigue tool also provides post-processing features, including fatigue damage contours, life estimates, and critical locations, to help the user identify potential failure locations and enhance the structure's design. All in all, the ANSYS fatigue tool is a useful software that can help improve the design and performance of engineering systems that have to handle repetitive loads.

3.4. Discussion

This chapter has focused on the procedures and phases used to carry out the current research. Discussing these methods in detail is crucial for understanding the design of examining the effect of bolts number and bolts size on fatigue life.

CHAPTER 4: RESULTS AND DISCUSSION

In this particular section, the results of the comprehensive analysis of the simulation study will be presented, wherein all cases will be carefully examined and evaluated. The outcomes of each scenario will be thoroughly discussed, to provide a more profound understanding of the obtained results.

4.1. Fatigue Life Results

The finite element models of the bolted connection were employed using ANSYS to determine the stresses and fatigue life of the bolt. The geometric properties were established based on the relevant normative standards, and the boundary conditions were modeled in accordance with the approach outlined in the methodology. This section presents and discusses the results obtained from the finite element simulation. The analysis provides insights into the behavior of the bolted connection under various loading conditions, including the stresses experienced by the bolt, the fatigue life of the connection, and any potential failure modes. The results are critical to evaluate the performance of the bolted flange connection and identifying potential areas of improvement. Table 9 summarizes all the fatigue life results for all different cases of the number of bolts and the sizes of bolts at all wind speeds. Table 9 summarizes the fatigue life results obtained from all scenarios that consider different numbers and sizes of bolts, across all wind speeds. These results provide critical insights into the performance of the bolted flange connection and can assist in determining the optimal configuration for the connection in terms of safety and durability.

Table 9. Fatigue Life result for all Cases.

	Fatigue Life (Cycles)											
Size of bolts	M36				M42				M48			
Wind speed / # Of Bolts	5m/s	10m/s	15m/s	20m/s	5m/s	10m/s	15m/s	20m/s	5m/s	10m/s	15m/s	20m/s
120	78071	14485	1765	614	139200	38273	3551	1208	286620	107540	7364	2416
140	115990	28222	2836	970	252240	97000	6599	2178	571360	260710	13594	4313
160	164530	47730	4354	1478	476820	168410	11466	3689	3333300	483070	24863	7264
180	232980	76827	6192	2049	765600	369670	18885	5685	3333300	764020	38856	10983
200	337130	122660	8504	2745	3333300	586640	29505	8593	N/A	N/A	N/A	N/A
220	476080	168110	11450	3685	N/A	N/A	N/A	N/A	N/A	N/A	N/A	N/A

To provide a more detailed understanding of these results, they will be illustrated and discussed using graphs. This approach will enable us to visualize the trends and variations in the fatigue life of the bolted flange connection across different scenarios, providing valuable insights into the behavior of the connection under all loading conditions.

4.1.1. Fatigue Life at 5 m/s average wind speed
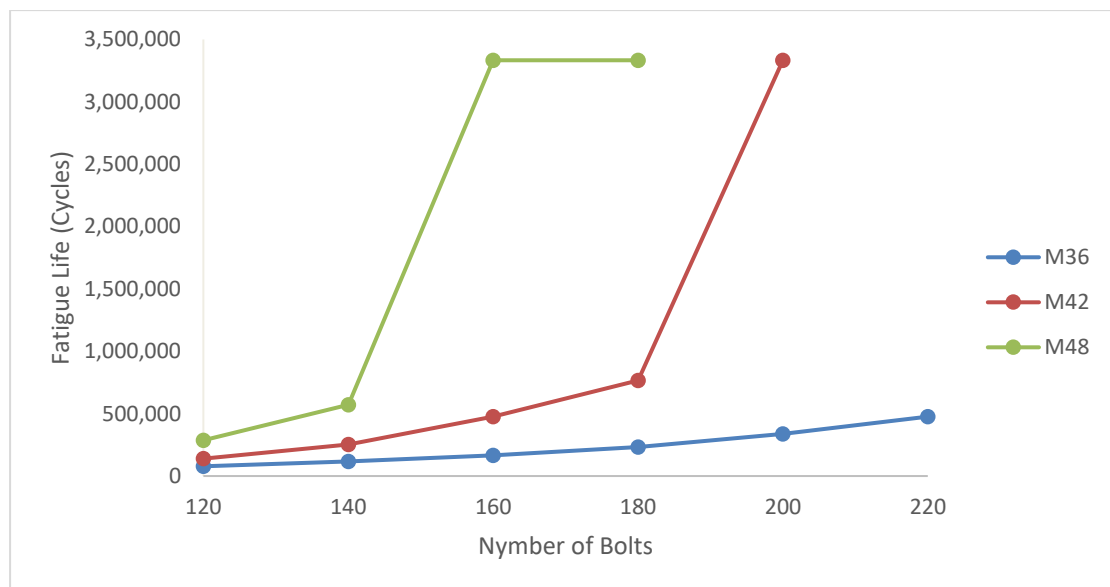
Figure 43. Fatigue Life vs the number of bolts for each bolt size at 5 m/s wind speed.

Figure 43 illustrates the fatigue life results at an average wind speed of 5 m/s for different numbers and sizes of bolts. The maximum fatigue life was observed using 160 M48 bolts and 200 M42 bolts. It can also be observed that for the M36 bolt, increasing the number of bolts improved the fatigue life of the flange significantly from 78,000 cycles to 476,000 cycles, but it did not reach its maximum potential compared to the other bolt sizes. Additionally, it can be seen that the slope at the end of the graph is steeper than the slope at the beginning, indicating that increasing the number of bolts

improves the fatigue life, but the improvement is not consistent for every 20 extra bolts. For the M42 bolt size, increasing the number of bolts slightly improved the fatigue life until a certain number of bolts were used, after which the fatigue life increased significantly. The M48 bolt exhibited a similar trend to the M42 bolt, reaching its peak fatigue life earlier.

Regarding the substantial rise discussed in the previous paragraph, it can be noticed that the M36 bolt size did not experience this rise, which indicates that fatigue will occur at this wind speed. However, the rise occurred in M42 and M48 bolts at two different points. For the M42 bolt size, the rise started after 180 bolts, meaning that the flange will reach its maximum fatigue life when the number of bolts exceeds 180. On the other hand, the M48 bolts started rising after they reached 140 bolts. Also, it is evident that increasing the number of bolts to more than 160 does not affect fatigue life. Therefore, the maximum fatigue life can be achieved in the 140 to 160 bolts range. The rise occurred between 140 and 160 bolts, which means that it may have occurred anywhere in this range. Therefore, it is recommended for the flange designer to investigate where exactly this rise occurs and design the flange accordingly to minimize the flange cost safely. Additionally, this graph clearly demonstrates that increasing the bolt size does increase fatigue life.

To determine the required fatigue life for this average speed, it is important to consider the location of the wind turbine. For instance, in Qatar, the average wind speed at 100 m elevation is around 5 m/s during the windier months of the year, which are November to April. Therefore, for this scenario, the maximum fatigue life is necessary. Based on this, it is essential to choose either 180+ M42 bolts or a range of 140 to 160 M48 bolts.

Figure 44. Fatigue Life vs the number of bolts for each bolt size at 10 m/s wind speed.

At the 10 m/s average wind speed, it is evident that increasing the number of bolts for M36 resulted in a significant increase in the flange's fatigue life, up to 1000%. Moreover, the slope was consistently positive for all cases, indicating that increasing the number of bolts would always enhance the fatigue life. For M42 bolt size, there was a slight increase in the fatigue life as the number of bolts increased. However, when the number of bolts reached a certain value, the fatigue life increased considerably.

The slope at the end of the curves for all bolt sizes is steeper, indicating that adding more bolts results in greater improvements in fatigue life. Specifically, for the M42 bolt size, fatigue life increases slightly with each additional bolt until it exceeds 160 bolts, after which it improves considerably. Similarly, for the M48 bolt size, fatigue life shows a significant increase after reaching 140 bolts.

Since this wind speed is rare in Qatar, a fatigue life of 150,000 cycles is recommended for the 10 m/s condition. Therefore, it is suggested to select the number of bolts either between 140 to 160 for M42 bolts or between 120 to 140 for M48 bolts.
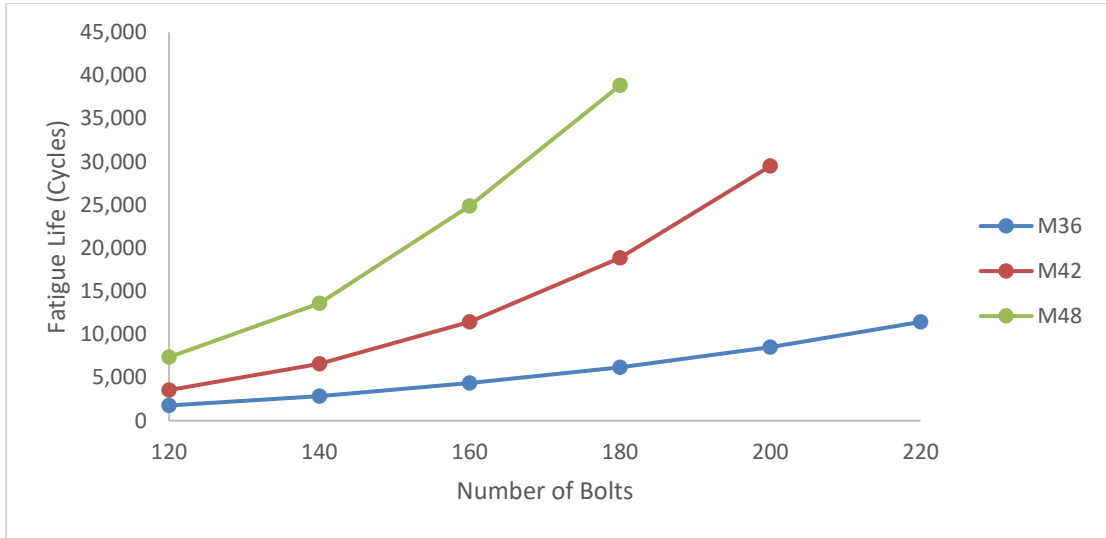
Figure 45. Fatigue Life vs number of bolts for each bolt size at 15 m/s wind speed.

The fatigue life cycles for the 15 m/s case are relatively low. However, it is important to note that 15 m/s is a high wind speed and occurs rarely. Based on Figure 45, the maximum fatigue life observed was approximately 40,000 cycles, while the minimum was 1,765 cycles, which is equivalent to 30 hours under these conditions.

The curves for all bolt sizes exhibit a positive slope, indicating an increase in fatigue life with the increasing number of bolts. However, the slope for M36 is the lowest compared to the other sizes. In contrast, M42 and M48 show very similar improvement slopes despite their different actual values. Furthermore, it is noticeable that the slope of the M42 curve increases significantly after an increment of 160 bolts, whereas the same trend occurs for M48 but after 140 bolts.

15 m/s is a high wind speed. If the user is designing a wind turbine in Qatar, 15,000 cycles fatigue life sounds reasonable. But if the user is designing for a different location, the number of cycles should be redesigned. In Qatar's case, the required bolt size and number can be easily observed from Figure 45, which is between 160 to 180 when using M42 and between 140 to 160 when using M48.
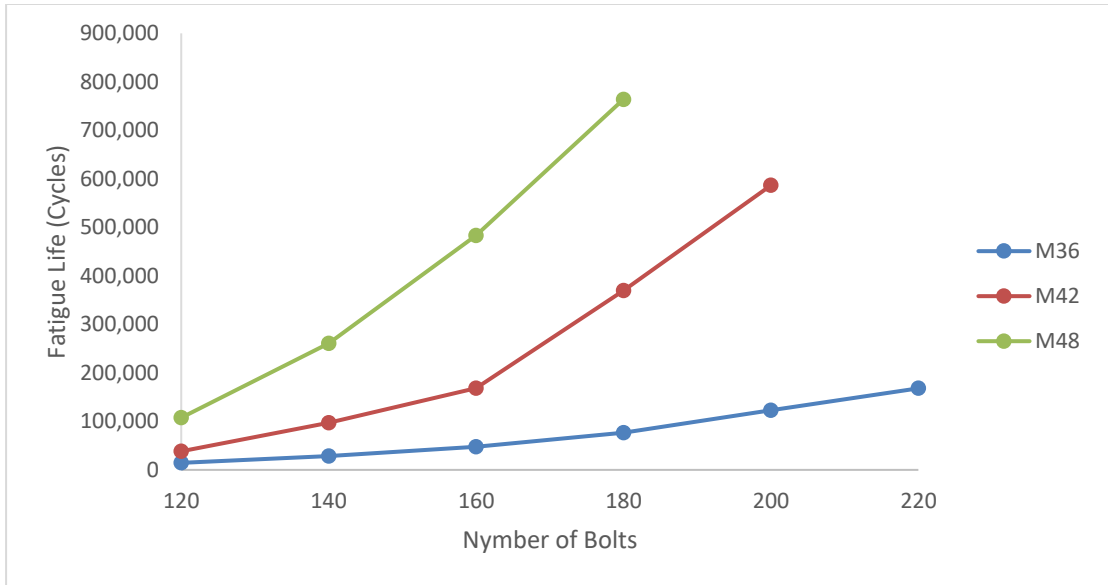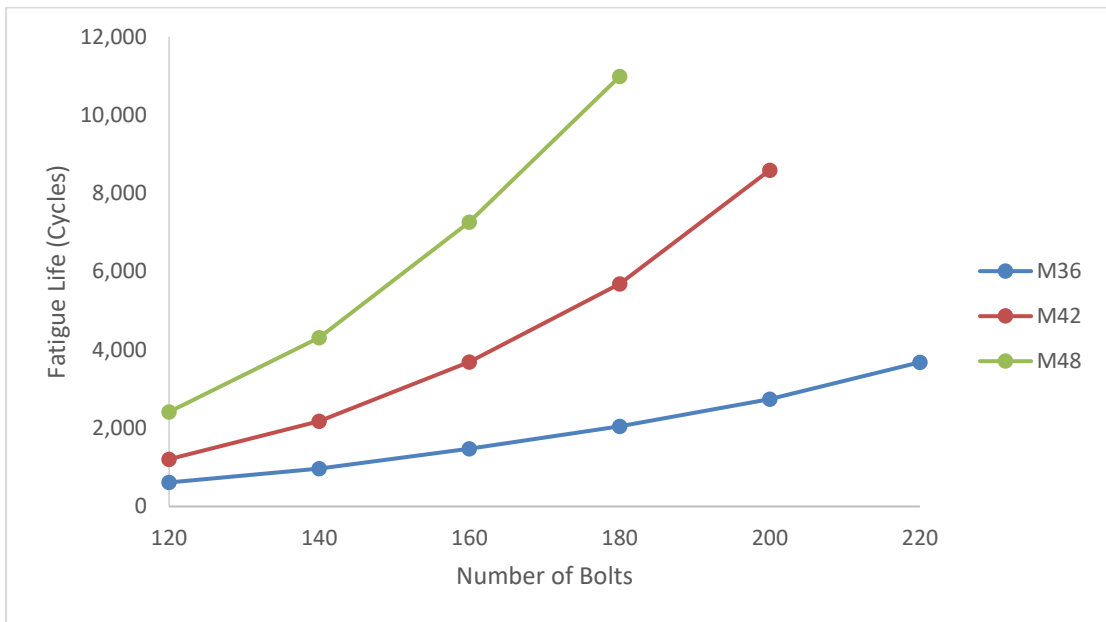
Figure 46. Fatigue Life vs the number of bolts for each bolt size at 20 m/s wind speed.

At an average wind speed of 20 m/s, increasing the number of bolts in all cases shows a slight improvement in the flange's fatigue life. Figure 46 also confirms that increasing bolt size or number improves the fatigue life of the flange.

The slope at the end is steeper than the slope at the beginning, indicating that adding more bolts will result in a greater improvement. Additionally, when comparing the M36 bolt to the M42 bolt, it can be observed that the rate of increment in the M42 slope is greater, indicating that adding larger bolts is more effective in improving fatigue life.

As 20 m/s is a very high wind speed and rarely occurs, the chosen fatigue life for this case is 5000 cycles. hence, the recommended number of bolts when using M42 ranges from 160 to 180, and, when using M48, ranges from 140 to 160.

4.1.5. Comparison of Fatigue Life at Different Wind Speeds

Comparing all the average speed results and for all bolt numbers and sizes the graphs show an improvement in the fatigue life whenever increasing the number of bolts or largening the bolt size. Unless reaching the maximum fatigue life of the material, then increasing the number of bolts or the size is impractical. In short, increasing the size of bolts or the number of bolts improves fatigue life.

Looking at all the curves' the slopes were positive, which proves that the studied cases improve fatigue life. Also, all the curves showed a steeper slope for the higher number of bolts, meaning that the increment percentage of adding bolts is not the same for every extra added bolt. Additionally, most figures showed that there is a noticeable improvement at some point for each size. For example, for the M42 bolt, this point is around 160 bolts. 5 m/s wind speed showed a unique behavior, none of the graphs had a rise in the same way as the one in it. This is simply the reason that the maximum fatigue life was not reached at any other wind speed, which knocks the idea of increasing the bolt sizes in a future study, since increasing the number of bolts is not feasible in all cases because of space limitations. The difference between the M48 and M42 bolts reaching the maximum life is almost 40 bolts. Unfortunately, this has not been confirmed to be a pattern since it wasn't possible to increase the number of bolts of the M36 to reach 240 bolts. one more interesting theoretical observation is that increasing the bolt size one step, is equivalent to adding 30 bolts of the same bolt size. this information can be tested in the future as well.

The desired fatigue life may vary depending on the location and preferences of the designer. Once the desired fatigue life is selected for each case, the designer can choose the intersection between the corresponding results to make their selection. For instance, the desired fatigue life varies based on the design location and user preference.

Using the chosen fatigue lives in this thesis, the corresponding bolt sizes for each case are 180 M42 bolts or 140 M48 bolts in the case of 5m/s, 160 for M42 or 140 for M48 bolts in the case of 10 m/s, 180 when using M42 or 160 when using M48 in the case of 15 m/s. And in the case of 20 m/s is 180 for M42 and 160 for M48, Therefore, the selected bolt size and number should be feasible in all cases, which amounts to either 180 M42 bolts or 160 M48 bolts.

4.2. Fatigue Life Improvement Percentage

The percentage of improvement in fatigue life varied across the different scenarios. Therefore, the following figures illustrate the percentage of improvement in fatigue life for each case, which will be discussed as well.

4.2.1. Improvement Percentage of Fatigue Life at 5 m/s average wind speed
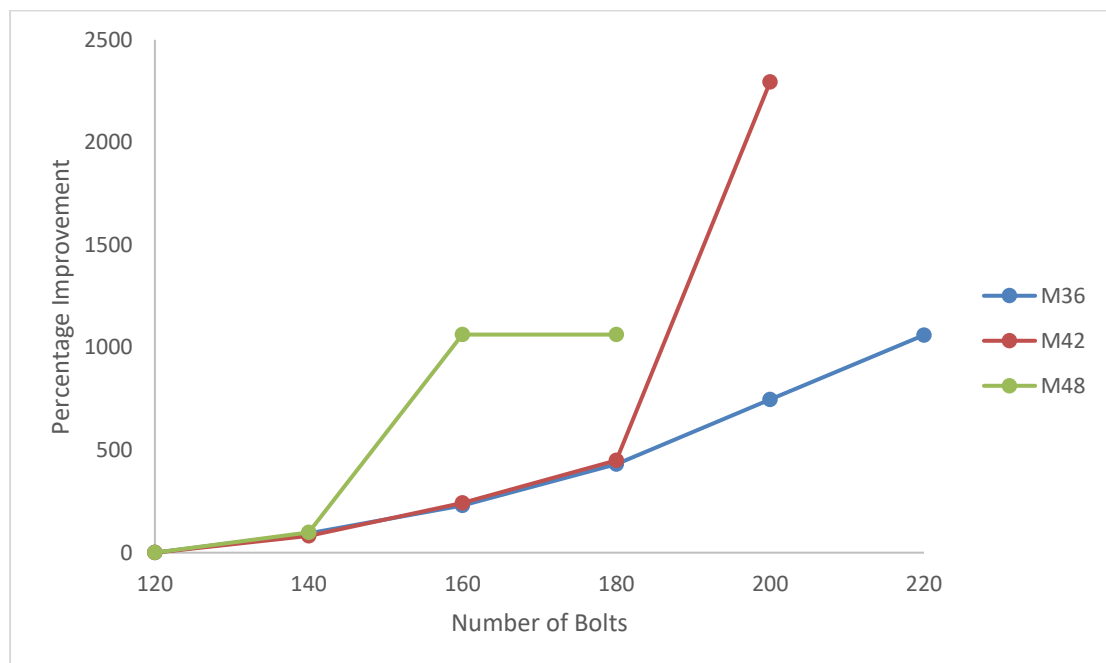
Figure 47. Fatigue Life improvement percentage at 5 m/s.

This figure illustrates the percentage improvement in fatigue life for all cases at an average wind speed of 5 m/s. The pattern of percentage improvements was consistent across all cases, with differences observed only when reaching the maximum fatigue life. Interestingly, adding the same number of bolts resulted in nearly identical percentage improvements.

4.2.2. Improvement Percentage of Fatigue Life at 10 m/s average wind speed
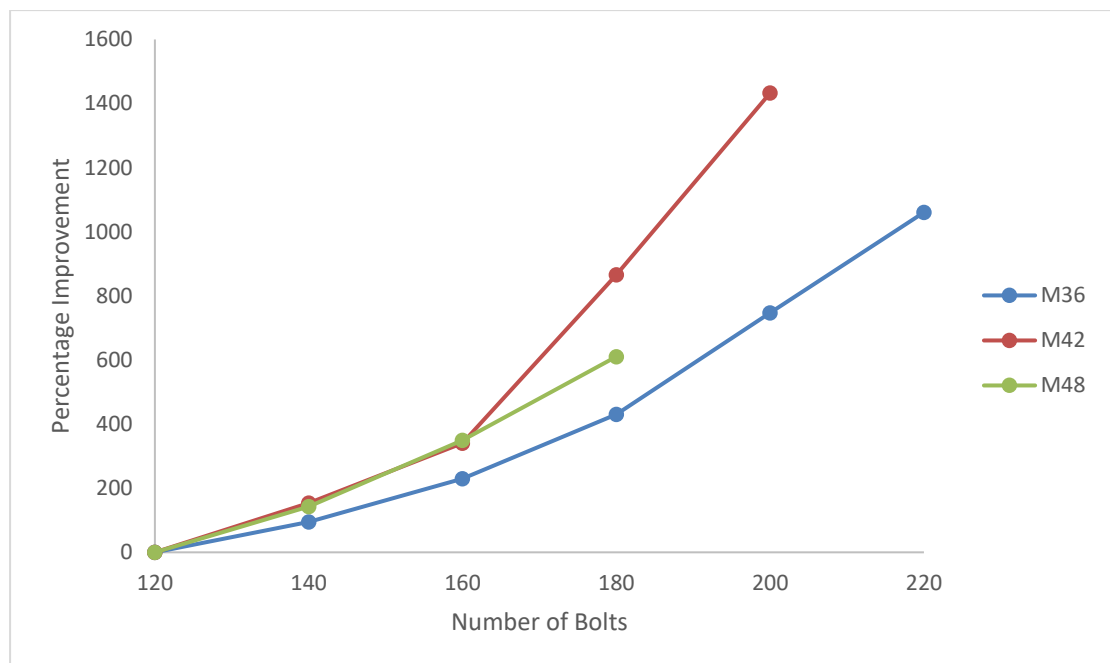
Figure 48. Fatigue Life improvement percentage at 10 m/s.

The graph in Figure 48 indicates that the improvement in fatigue life for M36 bolts is less than that for M42 and M48 bolts. However, it is not possible to generalize that increasing the bolt size increases the percentage improvement in fatigue life since the M42 and M48 bolts show similar improvement percentages for the first 40 additional bolts. Afterward, the improvement percentage for M42 bolts becomes greater than that for M48 bolts.
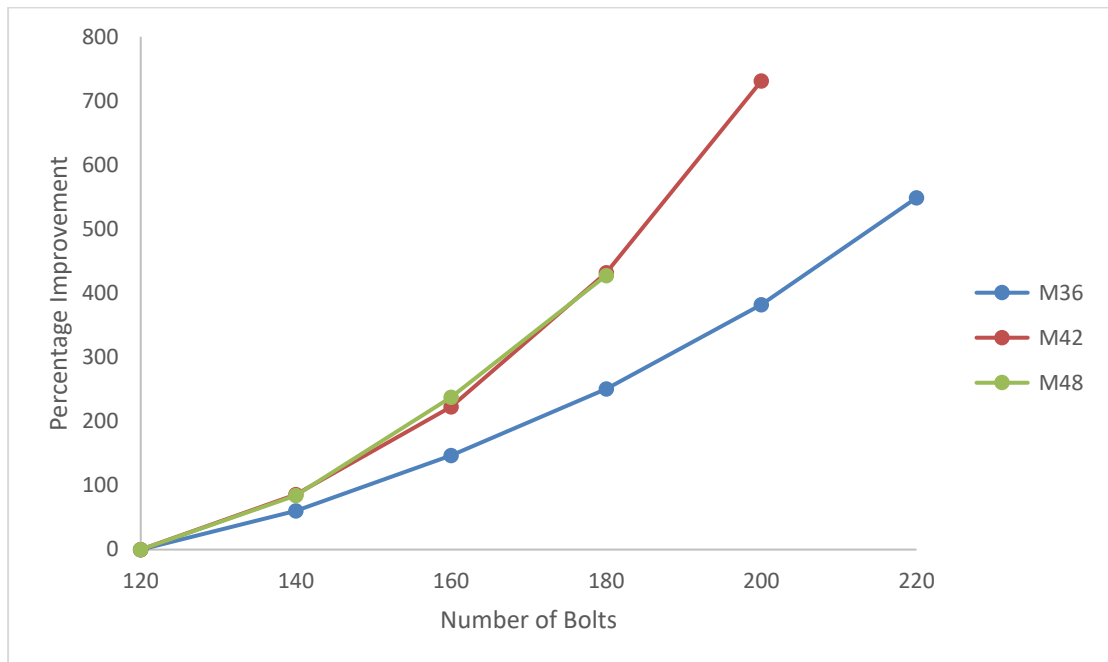
Figure 49. Fatigue Life improvement percentage at 15 m/s.

Figure 49 clearly illustrates that increasing the number of bolts results in similar percentage improvements for M48 and M42 bolts, indicating that both bolt types are equally effective in enhancing fatigue life. Additionally, the improvements observed for both M48 and M42 bolts are significantly higher than those achieved with M36 bolts.
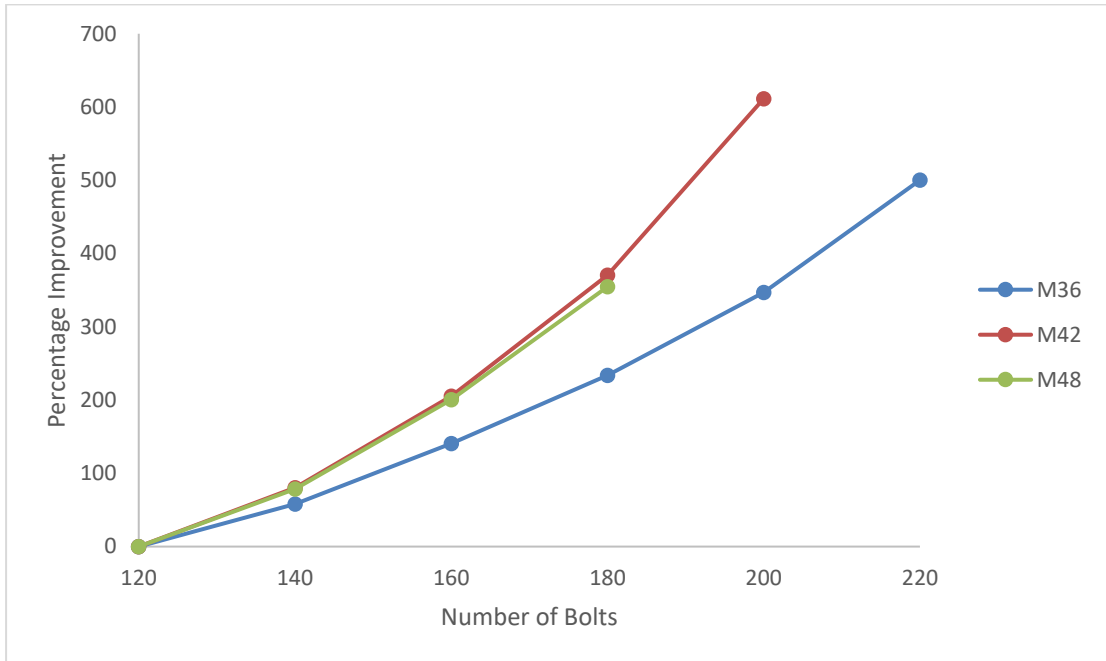
Figure 50. Fatigue Life improvement percentage at 20 m/s.

For the average speed wind of 20 m/s, the improvement percentage for the M36 bolts was less than the other sizes which are like the 10 m/s and 15m/s speeds. The difference here is that M42 showed a slightly higher improvement compared to the M48 which didn't happen in the 15 m/s case.

In all cases, M42 and M48 bolts showed nearly identical fatigue life improvement percentages. However, M36 bolts exhibited the same improvement behavior only when the average wind speed was 5 m/s, and this was before M42 and M48 bolts reached their maximum fatigue life. Moreover, as wind speed averages and loads increased, the improvement percentage of M36 bolts could not keep up with the other bolt sizes.

4.3. Fatigue Life Failure Location

From the results obtained by ANSYS it has been noticed that it is evident that fatigue failure occurs consistently at the same location between the bolt head and bolt shank, regardless of the bolt size or number. This finding highlights the importance of further research and improvements in this specific area to mitigate the occurrence of fatigue failure. The figures below are some samples of the results computed by ANSYS.

Figure 51. Stress in the bolts when using 120 M42 bolts at 5 m/s.
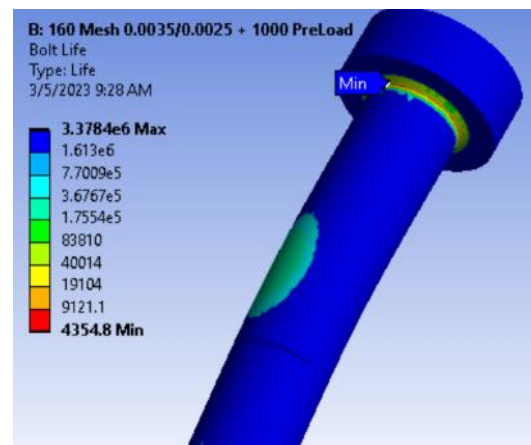
Figure 52. Stress in the bolts when using 160 M36 bolts at 15 m/s.
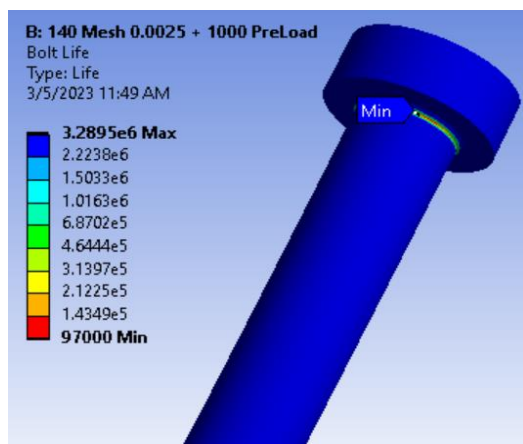
Figure 53. Stress in the bolts when using 140 M42 bolts at 10 m/s.
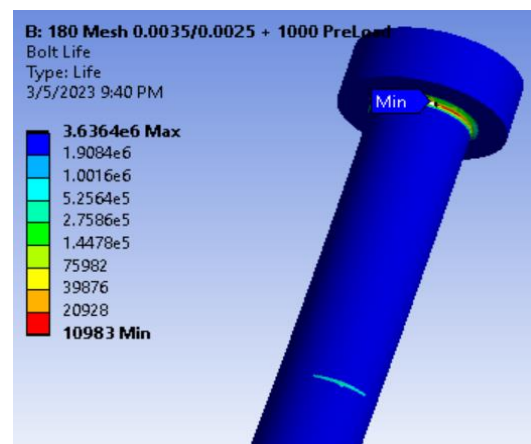
Figure 54. Stress in the bolts when using 180 M48 bolts at 20 m/s.

CHAPTER 5: CONCLUSION AND RECOMMENDATIONS

A thorough fatigue assessment was carried out on an L-flanged bolted connection using four distinct wind turbine simulation schemes. The wind turbines were exposed to averag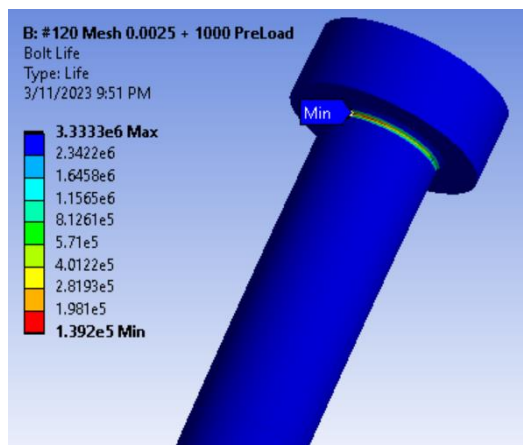e wind speeds of 5, 10, 15, and 20 m/s. The primary aim was to examine how the fatigue life was affected by increasing the number and size of bolts, while also developing a systematic methodology for analyzing the fatigue life of bolted flange connections more broadly.

5.1. Conclusion

After a thorough examination and analysis of the study results, several significant deductions and observations were made, leading to the following conclusions.

1- Increasing the size or number of bolts can significantly enhance the fatigue life of bolted flange connections.

2- the percentage increment of adding bolts is not consistent for every additional bolt. Instead, the curves plotted from the data reveal a steeper slope for a larger number of bolts, indicating an exponential increase in the percentage increment with an increasing number of bolts.

3- the most suitable design improvement approach varies depending on the circumstances. It is important to consider the specific situation, as increasing the number of bolts may not always be a viable option due to spatial limitations.

4- In most scenarios, M42 and M48 bolts displayed nearly identical improvement percentages when adding the same number of bolts. This finding can be useful in determining the most cost-effective solution for improving fatigue life.

5- Additionally, a noteworthy theoretical observation was made that increasing the

bolt size by one level is equivalent to adding thirty bolts of the same size. This observation can aid in predicting the impact of changes in bolt size on fatigue life, which can be useful in the design process.

5.2. Recommendations for Future Work

To improve the fatigue life of bolted connections and mitigate the occurrence of fatigue failure, several areas of further research and study can be explored. These areas may include:

1. Exploring the effects of using different materials for bolts, such as high-carbon steel, on the fatigue life of bolted connections.

2. Investigating the effects of using different numbers of bolts on the fatigue life of bolted connections to determine the optimum number for improved performance.

3. Examining the effects of using larger bolt sizes on the fatigue life of bolted connection to determine if they are going to reach the maximum fatigue life.

4. Analyzing the effects of different bolt preloads on the fatigue life of bolted connections.

5. Studying the range at which the fatigue life reaches its maximum to determine where it occurs precisely.

6. Investigating the effects of adding different bolt sizes to bolted flanges on the fatigue life.

By exploring these areas, we can gain a deeper understanding of the factors that contribute to fatigue failure in bolted connections and identify ways to improve their performance.

REFERENCES

[1] "8.1 Renewable Energy Basics | EME 807: Technologies for Sustainability Systems." https://www.e-education.psu.edu/eme807/node/649 (accessed Jun. 02, 2023).

[2] A. Habte *et al.*, "Developing a Framework for Reference Cell Standards for PV Resource Developing a Framework for Reference Cell Standards for PV Resource Applications," no. January 2019, 2018.

[3] H. Zhang, J. Cai, K. Fang, F. Zhao, and J. W. Sutherland, "Operational optimization of a grid-connected factory with onsite photovoltaic and battery storage systems," *Appl. Energy*, vol. 205, pp. 1538–1547, Nov. 2017, doi: 10.1016/J.APENERGY.2017.08.140.

[4] Y. Lee, S., Kim, J., & Kim, "Public perception and acceptance of photovoltaic systems," *Renew. Energy*, vol. 134, pp. 225–232, 2019.

[5] A. M. M. Liu, O. X. Liang, M. Tuuli, and I. Chan, "Role of government funding in fostering collaboration between knowledge-based organizations: Evidence from the solar PV industry in China," *Energy Explor. Exploit.*, vol. 36, no. 3, pp. 509–534, May 2018, doi: 10.1177/0144598717742968/ASSET/IMAGES/LARGE/10.1177_0144598717 742968-FIG2.JPEG.

[6] Y. Gao, J., Li, X., & Zhang, "Design and optimization of wind turbines," *Renew. Energy*, vol. 112, pp. 95–105, 2018.

[7] Y. Chen, X., Liu, Y., & Wang, "The impact of wind energy on local communities," *Renew. Energy*, vol. 121, pp. 128–137, 2018.

[8] World Energy Council, "Hydropower," 2019.

[9] Y. Li, X., Liu, Y., & Wang, "The impact of hydro energy on local communities,"

Renew. Energy, vol. 121, pp. 138–147, 2018.

[10]   J. Zhang, Y., Li, H., Zhang, Q., & Li, "Geothermal energy: A review on sustainable approaches for its utilization," *Renew. Sustain. Energy Rev.*, vol. 101, pp. 627–640, 2019.

[11]   J. Li, X., Zhang, Y., & Gao, "Design and optimization of geothermal power plants," *Renew. Energy*, vol. 134, pp. 233–240, 2019.

[12]   R. K. Dixit, M. K., Das, P., & Gupta, "Biomass energy and environment: A review.," *Renew. Sustain. Energy Rev.*, vol. 145, 2021.

[13]   S. M. Rozainee, M. N., Mohamad, M. F., & Shafie, "Overview on the potential of biomass energy for sustainable electricity generation in Malaysia.," *Renew. Sustain. Energy Rev.*, vol. 119, 2020.

[14]   C. Mubofu, E. B., Simbizi, R. N., & Mbohwa, "Biomass energy in the circular economy: A review.," *Renew. Sustain. Energy Rev.*, vol. 137, 2021.

[15]   S. Younossi, O., & Zeyghami, *Wind energy fundamentals, resource analysis and economics*. Springer, 2015.

[16]   N. Jørgensen, J. H., & Skou, *Wind turbine technology: Principles and design*. 2008.

[17]   L. R. Ivan Komusanac, Guy Brindley, Daniel Fraile, "Wind energy in Europe 2020 Statistics and the outlook for 2021-2025," *windeurope.org*, pp. 1–37, 2021, [Online]. Available: https://windeurope.org/intelligence-platform/product/wind-energy-in-europe-in-2020-trends-and-statistics/%0Afile:///C:/Users/kübra/Desktop/tezler/210224_windeurope_combined_2020_stats.pdf

[18]   A. L. John Wiley & Sons. Manwell, J. F., McGowan, J. G., & Rogers, *Wind energy explained: Theory, design and application*. 2002.

[19] P. John Wiley & Sons. Musgrove, *A history of wind turbines*. Shire Publications, 2014.

[20] National Renewable Energy Laboratory, "Best locations for wind turbines," 2018. https://www.nrel.gov/workingwithus/re-wind-best-locations.html

[21] European Wind Energy Association, "The challenges of wind energy," 2021. https://www.ewea.org/the-challenges-of-wind-energy/

[22] American Wind Energy Association, "Environmental impact of wind energy," 2019. https://www.awea.org/environmental-impact-wind-energy

[23] C. Bak, "Aerodynamic design of wind turbine rotors," *Adv. Wind Turbine Bl. Des. Mater.*, pp. 59–108, Jan. 2013, doi: 10.1533/9780857097286.1.59.

[24] M. F. Jensen and K. Branner, "Introduction to wind turbine blade design," *Adv. Wind Turbine Bl. Des. Mater.*, pp. 3–28, Jan. 2013, doi: 10.1533/9780857097286.1.3.

[25] Q. Liu, X., Liu, Y., Zhang, Q., & Yang, "Design optimization of wind turbine rotor blade using a novel hybrid method," *Energy*, vol. 154, pp. 356–365, 2018.

[26] X. Zhang, Y., Li, Y., & Zhang, "Design and optimization of wind turbine rotor blade based on CFD analysis," *J. Renew. Energy*, vol. 12, no. 3, pp. 333–342, 2020.

[27] R. Otero, J., Domingo, P., & Otero, "Review of wind turbine generator technologies," *Renew. Energy*, vol. 126, pp. 15–29, 2019.

[28] A. Pouliezos, "Wind Turbine Control Systems and Power Electronics," *Compr. Renew. Energy*, vol. 2, pp. 329–370, Jan. 2012, doi: 10.1016/B978-0-08-087872-0.00212-2.

[29] Z. Wang, Y., Cui, Z., & Zhang, "Study on generator systems for wind turbines," *J. Clean Energy Technol.*, vol. 9, no. 2, pp. 93–100, 2021.

[30]   Z. Zemali *et al.*, "Robust intelligent fault diagnosis strategy using Kalman observers and neuro-fuzzy systems for a wind turbine benchmark," *Renew. Energy*, vol. 205, pp. 873–898, Mar. 2023, doi: 10.1016/J.RENENE.2023.01.095.

[31]   X. Zheng, L., Chen, Y., & Zhang, "Development of wind turbine control systems," *J. Clean Energy Technol.*, vol. 8, no. 2, pp. 77–85, 2020.

[32]   Q. Yang, Y. Li, T. Li, X. Zhou, G. Huang, and J. Lian, "Statistical extrapolation methods and empirical formulae for estimating extreme loads on operating wind turbine towers," *Eng. Struct.*, vol. 267, p. 114667, Sep. 2022, doi: 10.1016/J.ENGSTRUCT.2022.114667.

[33]   Y. Tao, W., Gao, J., & Liu, "Tower design of large wind turbines: A review," *Energy*, vol. 170, pp. 700–716, 2019.

[34]   Y. Wu, Y., Liu, X., & Wei, "A review of tower materials for wind turbines," *J. Renew. Energy*, vol. 11, no. 5, pp. 726–732, 2018.

[35]   T. Wang, Z. Zhang, J. Zhang, Z. Chen, J. Xian, and L. Zhang, "Performance-based assessment of the monopile foundation of offshore wind turbines," *Ocean Eng.*, vol. 266, p. 113083, Dec. 2022, doi: 10.1016/J.OCEANENG.2022.113083.

[36]   Y. Guo, P. Zhang, H. Ding, and C. Le, "Design and verification of the loading system and boundary conditions for wind turbine foundation model experiment," *Renew. Energy*, vol. 172, pp. 16–33, Jul. 2021, doi: 10.1016/J.RENENE.2021.03.017.

[37]   Q. Liu, X., Liu, Y., Zhang, Q., & Yang, "Analysis of flange design for wind turbine tower mid-connection," *J. Clean Energy Technol.*, vol. 8, no. 4, pp. 215–221, 2020.

[38] X. Zhang, Y., Li, Y., & Zhang, "Design and analysis of gusset plates for wind turbine tower mid-connection," *J. Renew. Energy*, vol. 12, no. 3, pp. 276–283, 2020.

[39] X. Chen, Y., Liu, X., & Zhang, "Study of bolts for wind turbine tower mid-connection," *J. Renew. Energy*, vol. 13, no. 2, pp. 167–174, 2021.

[40] Y. Yue *et al.*, "Applicability Analysis of Inspection and Monitoring Technologies in Wind Turbine Towers," *Shock Vib.*, vol. 2021, 2021, doi: 10.1155/2021/5548727.

[41] M. Alonso-Martinez, J. M. Adam, F. P. Alvarez-Rabanal, and J. J. del Coz Díaz, "Wind turbine tower collapse due to flange failure: FEM and DOE analyses," *Eng. Fail. Anal.*, vol. 104, pp. 932–949, Oct. 2019, doi: 10.1016/J.ENGFAILANAL.2019.06.045.

[42] Y. Zhang, J., Zhou, L., & Chen, "Investigation of the causes of flange connection failures in wind turbine towers," *J. Renew. Energy*, vol. 158, pp. 934–939, 2021.

[43] Q. Liu, Y., Zhang, Y., & Chen, "Analysis of the cause of flange connection failure in wind turbine tower," *J. Clean Energy Technol.*, vol. 8, no. 5, pp. 569–573, 2020.

[44] Z. Wang, Y., Chen, Z., & Chen, "Study on the fatigue failure of flange connection in wind turbine tower," *J. Renew. Energy*, vol. 156, pp. 937–942, 2021.

[45] D. Croccolo, M. De Agostinis, S. Fini, G. Olmi, F. Robusto, and C. Scapecchi, "Fretting Fatigue in Mechanical Joints: A Literature Review," *Lubr. 2022, Vol. 10, Page 53*, vol. 10, no. 4, p. 53, Mar. 2022, doi: 10.3390/LUBRICANTS10040053.

[46] R. Eichstädt, "Fatigue assessment of large-size bolting assemblies for wind

turbine support structures," 2019, doi: 10.15488/5157.

[47] "EN 1993-1-8: Eurocode 3: Design of steel structures - Part 1-8: Design of joints".

[48] S. M. Hosseini, F. Mashiri, and O. Mirza, "Fatigue performance of bolted shear connectors," *Aust. J. Struct. Eng.*, vol. 23, no. 1, pp. 59–74, 2022, doi: 10.1080/13287982.2021.1999010.

[49] Z. Jiang, S. Wan, Z. Fang, and A. Song, "Static and fatigue behaviours of a bolted GFRP/steel double lap joint," *Thin-Walled Struct.*, vol. 158, Jan. 2021, doi: 10.1016/J.TWS.2020.107170.

[50] P. Schaumann, R. Eichstädt, and A. Stang, "Advanced performance assessment methods for high-strength bolts in ring-flange connections," *Stahlbau*, vol. 87, no. 5, pp. 446–455, May 2018, doi: 10.1002/STAB.201810601.

[51] J. Jorgensen, M. Hodkiewicz, E. Cripps, and G. M. Hassan, "Predicting Bolt Stress Under Uncertainty in Offshore Wind Turbine Structural Connections Using a Gaussian Process Surrogate Model," pp. 477–484, Jun. 2021, doi: 10.26182/31HP-TD58.

[52] Z. Kapidžić, "Comparison of fatigue life and flexibility between aluminum-composite and aluminum–aluminum bolted joints," *Int. J. Fatigue*, vol. 157, p. 106695, Apr. 2022, doi: 10.1016/J.IJFATIGUE.2021.106695.

[53] D. Radaj, C. M. Sonsino, and W. Fricke, *Fatigue Assessment of Welded Joints by Local Approaches: Second Edition*. Elsevier Ltd, 2006. doi: 10.1533/9781845691882.

[54] D. Radaj and M. Vormwald, "Advanced methods of fatigue assessment," *Adv. Methods Fatigue Assess.*, vol. 9783642307409, pp. 1–490, May 2013, doi: 10.1007/978-3-642-30740-9.

[55]   D. and M. Socie, "Multiaxial fatigue," *Soc. Automot. Eng.*, p. 129, 2000.

[56]   P. Schaumann and R. Eichstädt, "Fatigue Assessment of High-Strength Bolts with Very Large Diameters in Substructures for Offshore Wind Turbines," 2015, Accessed: Feb. 27, 2023. [Online]. Available: www.isope.org

[57]   Q. Wang, M. Kashif Khan, and C. Bathias, "Current understanding of ultra-high cycle fatigue," *Theor. Appl. Mech. Lett.*, vol. 2, p. 31002, 2012, doi: 10.1063/2.1203102.

[58]   B. Pyttel, D. Schwerdt, and C. Berger, "Very high cycle fatigue – Is there a fatigue limit?," *Int. J. Fatigue*, vol. 33, no. 1, pp. 49–58, Jan. 2011, doi: 10.1016/J.IJFATIGUE.2010.05.009.

[59]   J. Toribio *et al.*, "Fatigue behaviour of bolted joints," *MMI*, vol. 18, no. 4, pp. 553–558, 2012, doi: 10.1007/S12540-012-4001-3.

[60]   I. Marines, X. Bin, and C. Bathias, "An understanding of very high cycle fatigue of metals," *Int. J. Fatigue*, vol. 25, no. 9–11, pp. 1101–1107, Sep. 2003, doi: 10.1016/S0142-1123(03)00147-6.

[61]   A. Wang, Z. Wang, Y. Zhao, Z. Chang, X. Shao, and Y. Kang, "Fatigue behaviour and failure mechanism of the thin/thick-ply hybrid laminated composite bolted joints," *Compos. Struct.*, vol. 295, Sep. 2022, doi: 10.1016/J.COMPSTRUCT.2022.115636.

[62]   R. S. Charlton, "Threaded fasteners: Part 1 - Failure modes and design criteria of connections," *NACE - Int. Corros. Conf. Ser.*, Jan. 2011.

[63]   E. Haibach, "Modified linear damage accumulation hypothesis accounting for a decreasing fatigue strength during increasing fatigue damage," *Darmstadt Lab. f¨ur Betriebsfestigkeit, LBF.*, 1970.

[64]   P. Schaumann and D.-I. Frithjof Marten, "Fatigue Resistance of High Strength

Bolts with Large Diameters".

[65] S. Lochan, A. Mehmanparast, and J. Wintle, "A review of fatigue performance of bolted connections in offshore wind turbines," *Procedia Struct. Integr.*, vol. 17, pp. 276–283, Jan. 2019, doi: 10.1016/J.PROSTR.2019.08.037.

[66] B. Eccles, "Fatigue Failure of Bolts", Accessed: Feb. 27, 2023. [Online]. Available: www.boltscience.co.uk.

[67] T. Matsunari, K. Oda, N. Tsutsumi, T. Yakushiji, N. A. Noda, and Y. Sano, "Experimental study on the effect of shape of bolt and nut on fatigue strength for bolted joint," *MS&E*, vol. 372, no. 1, p. 012016, Jun. 2018, doi: 10.1088/1757-899X/372/1/012016.

[68] M. T. Hinds, "Bolted joint design: the basics.," *Machine Design*, 2017. https://www.machinedesign.com/mechanical-motion-systems/article/21833674/bolted-joint-design-the-basics

[69] Y. ZUO, T. YUE, R. JIANG, Z. CAO, and L. YANG, "Bolt insertion damage and mechanical behaviors investigation of CFRP/CFRP interference fit bolted joints," *Chinese J. Aeronaut.*, vol. 35, no. 9, pp. 354–365, Sep. 2022, doi: 10.1016/J.CJA.2022.01.027.

[70] Y. L. Lee and T. Tjhung, "Rainflow Cycle Counting Techniques," *Met. Fatigue Anal. Handb.*, pp. 89–114, 2012, doi: 10.1016/B978-0-12-385204-5.00003-3.

[71] A. International, "E 1040-85 - Standard Practices for Cycle Counting in Fatigue Analysis," 2005.

[72] A. Zangouie, L. D. Wegner, and J. Muthu, "Fretting Fatigue Characterization of Bolted Steel Connections with Different Surface Treatments," *Lect. Notes Civ. Eng.*, vol. 244, pp. 173–184, 2022, doi: 10.1007/978-981-19-0656-5_15.

[73] M. M. Pedersen, "Introduction to Metal Fatigue: Concepts and Engineering

Approaches," *Tech. Rep. Mech. Eng.*, vol. 5, no. 11, p. 91, Nov. 2018, Accessed: Feb. 27, 2023. [Online]. Available: https://tidsskrift.dk/me/article/view/110952

[74] O. Kalan, "Fatigue Life Assessment of 5 Mw Onshore Wind Turbines," no. August 2012, 2012.

[75] "Global Wind Atlas." https://globalwindatlas.info/en (accessed Jun. 02, 2023).

[76] B. Jonkman, "Turbsim user's guide v2. 00.00," *Natl. Renew. Energy Lab*, 2014.

[77] B. J. Jonkman and J. M. Jonkman, "FAST v8.16.00a-bjj User's Guide," *Nrel*, p. 58, 2016.

[78] V. Sadananda, K., & Ramaswamy, "Fatigue behavior of steels," in *ASM Handbook*, 1996, pp. 466–483.

[79] J. Schijve, "Fatigue behavior of steel structures," *Fatigue Des. steel Compos. Struct.*, pp. 3–19, 2011.

[80] J. Braithwaite and A. Mehmanparast, "Analysis of Tightening Sequence Effects on Preload Behaviour of Offshore Wind Turbine M72 Bolted Connections," *Energies 2019, Vol. 12, Page 4406*, vol. 12, no. 23, p. 4406, Nov. 2019, doi: 10.3390/EN12234406.

[81] S. Sahin, S., & Kilic, "Effect of surface roughness on friction and wear behavior of aluminum alloy and structural steel sliding against polyurethane," *Wear*, pp. 324–325, 148-155., 2015.

[82] L. Zhang, W., Guo, Y., Zhang, J., & Ma, "Comparative study of single-zone and multizone mesh methods for simulating dynamic responses of pavement structures," *J. Test. Eval.*, vol. 44, no. 1, pp. 148–154, 2015.